CENTRO DE INVESTIGACIÓN Y DE ESTUDIOS AVANZADOS
DEL INSTITUTO POLITÉCNICO NACIONAL
UNIDAD QUERÉTARO

Cinvestav-Querétaro

La estructura de películas de pentaceno crecidas en substratos de Au y TaN

Tesis que presenta

Maribel Maldonado García

Para obtener el grado de

Maestro en Ciencias

en la Especialidad de

Materiales

Director de Tesis:

Dr. Alberto Herrera Gómez

Codirector de Tesis:

Dr. Rafael Ramírez Bon

Santiago de Querétaro, Qro.   **Noviembre del 2007**
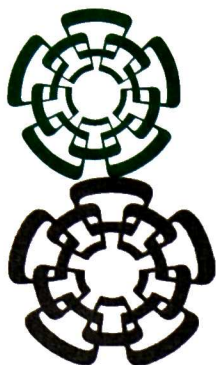
CENTRO DE INVESTIGACION Y DE ESTUDIOS AVANZADOS DEL I.P.N.

CENTRO DE INVESTIGACIÓN Y DE ESTUDIOS AVANZADOS
DEL INSTITUTO POLITÉCNICO NACIONAL
UNIDAD QUERÉTARO

Cinvestav-Querétaro

The structure of pentacene films grown on Au and TaN substrates

Thesis presented by

Maribel Maldonado García

To obtain the degree of

Master of Science
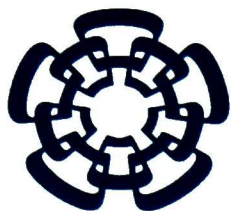
In

Materials Science

Thesis Director:

Dr. Alberto Herrera Gómez

Thesis Co-director:

Dr. Rafael Ramírez Bon

Santiago de Querétaro, Qro.   November 2007

CENTRO DE INVESTIGACIÓN Y DE ESTUDIOS AVANZADOS
DEL INSTITUTO POLITÉCNICO NACIONAL
UNIDAD QUERÉTARO

Cinvestav-Querétaro

The Structure of Pentacene Films Grown on Au and TaN Substrates

Tesis que presenta

Maribel Maldonado García

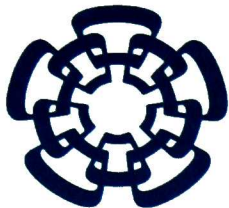Para obtener el grado de

Master of Science

On

Materials Science

Directores de Tesis:

Dr. Alberto Herrera Gómez
Dr. Rafael Ramírez Bon

Santiago de Querétaro, Qro.   Noviembre 2007

CENTRO DE INVESTIGACIÓN Y DE ESTUDIOS AVANZADOS
DEL INSTITUTO POLITÉCNICO NACIONAL
UNIDAD QUERÉTARO

Cinvestav-Querétaro

La estructura de películas de pentaceno crecidas en nitruro de tantalio y oro.

Tesis que presenta

Maribel Maldonado García

Para obtener el grado de

Maestro en Ciencias

en la Especialidad de

Materiales

Directores de Tesis:

Dr. Alberto Herrera Gómez
Dr. Rafael Ramírez Bon

Santiago de Querétaro, Qro.   Noviembre 2007

A la familia Maldonado García

A A. Vidal

Nunca es tarde para empezar , nunca es tarde para pedir perdón. No le tengas miedo al miedo tenle miedo a tu propia cobardía, no habrá peor daño que el que tú mismo te hagas.; Solo venciéndote a ti mismo vencerás a los demás.

Agradecimientos

A los profesores que nos apoyaron con la flexibilidad de su tiempo y las facilidades otorgadas durante nuestra estancia: Dr. Trápaga, Dr. Manzano y Dr. Rafael. Sin olvidar al Ing. Omar Castillo por el apoyo durante la transmisión de las clases.

A todos mis profesores por haber sembrado en mi la semilla de la investigación.

A Conacyt por su ayuda económica, y apoyo a la realización de este trabajo.

Acknowlededgments

A journey is easier when you travel together. Interdependence is certainly more valuable than independence. This thesis is the result of two years of work whereby I have been accompanied and supported by many people. It is a pleasant aspect that I have now the opportunity to express my gratitude for all of them.

I am profoundly indebted to Dr. Bruce Gnade who could not be listed as advisor but without his support I could have not initiated or developed my thesis work.

From the formative stages of this thesis, to the final draft, I owe an immense debt of gratitude to my advisor, Dr. Alberto Herrera. His sound advice and careful guidance were invaluable in this thesis.

This work would not have been possible without the support and encouragement of my boss and friend; Dr. Francisco Servando, under whose supervision I Face the problems in my work.

To Dr. Manuel Quevedo for his advisor, in the final stages of my work, has also been abundantly helpful, and has assisted me in numerous ways. Thanks for your time and your guidance in this thesis.

My former colleagues from Cinvestav that supported me in my research work. I want to thank them for all their help, support, interest and valuable hints. Especially I am obliged to Daniela Morales, Isabel Medina , and Rocio Contreras that make my USA stay the best experience. And my friends who even with the distance were all time with me thanks Pilar Montellano and Luis Morales.

Acronyms

- AFM   Atomic Force Microscopy
- ARXPS   Angle Resolved X-Ray Photoemission Spectroscopy
- CA   Contact Angle
- FTIR   Fourier Transmission Infrared Spectroscopy
- HMDS   Hexamethyldisilazane
- HOMO   Highest Occupied Molecular Orbital
- LUMO   Lower Unocupied Molecular Orbital
- ML   Monolayer
- OTFT   Organic Thin Films Transistors
- PAH   Polycyclic Aromatic Hydrocarbon
- Ra   Roughness Average
- RCA   Radio Corporation of America
- RMS   Roughness Mean Square
- SC   Standard Cleaning
- SDBS   Spectra Database for Organic Compounds
- TI   Texas Instruments Company
- XPS   X-Ray Photoemission Spectroscopy
- XRD   X-ray Diffraction
- UHV   Ultra-High Vacuum
- UPS   Ultra Violet Photoemission Spectroscopy
- UV-Ozone   Ultra Violet Ozone cleaning
- WF   Work Function

Outline

List of tables

List of Figures

Resumen

El desarrollo de electrónica flexible es de gran interés, y los materiales orgánicos son clave en estos dispositivos. En la fabricación de Transistores de Películas Delgadas de Orgánicos (OTFT, por sus siglas en inglés), el pentaceno se ha convertido en la opción por su alta movilidad (tipo p). Debido a su función de trabajo (~5 eV), el oro (Au) es normalmente usado como contacto en los OTFT. El nitruro de tantalio (TaN) tiene una función de trabajo similar a la del oro. Implementando TaN como contacto en los OTFTs el costo de proceso se podría reducir considerablemente. En el presente trabajo las interacciones químicas de Pentaceno en oro y Pentaceno en TaN fueron investigadas a utilizando métodos de caracterización como espectroscopía de fotoemisión de rayos-x (XPS), XPS resuelto en el ángulo, espectroscopía de infrarrojo (FTIR), microscopia de fuerza atómica (AFM), difracción de rayos x (XRD), entre otros. Se caracterizó el impacto en la estructura de las películas de pentaceno del substrato y de su temperatura, así como la adición de una película de Hexamethyldisilazane (HMDS) como intercapa entre el metal y el pentaceno. De este estudio fue posible desechar la asociación de una de las componentes químicas del pentaceno en el enlace con el Au o el TaN. Para ambos substratos, cuando la película de pentaceno se creció a 55°C se formaron grandes agregados que no cubrieron toda la superficie, aún para películas de pentaceno nominalmente gruesas. Para esa temperatura la rugosidad de las películas fueron del orden de su espesor. La morfología fue muy dependiente del substrato. Mientras que en oro el pentaceno creció en modo dendrítico, en TaN el pentaceno se agregó alrededor de puntos distribuidos en la superficie. En contraste con el TaN, el HMDS no se adhirió al oro; sin embargo, el tratamiento afectó el crecimiento del pentaceno al cambiar el carácter hidrofóbico de la superficies. Su efecto en la morfología fue sutil pero detectable. Cuando el substrato fue tratado con HMDS, los granos del pentaceno mostraron más estructura. En el caso del oro, el HMDS causó que el crecimiento del pentaceno fuera más direccional.

El trabajo experimental fue realizado en su totalidad en The University of Texas at Dallas, dentro del Materials Science Group de la Erik Johsson School of Engineering and Computer Science.

Abstract

The use of organic materials for flexible electronic devices is of paramount importance. For Organic Thin Film Transistors (OTFT), pentacene has become the most promising material due to its high hole mobility. Due to its large work function (~5 eV), Au_is normally used as the charge injecting electrode. TaN also has a work function similar to Au. Using TaN as the electrode could reduce costs during processing. In this work, the pentacene/Au and pentacene/TaN interfaces were investigated through X-Ray Photoemission Spectroscopy (XPS), Angled Resolved XPS, Fourier Transform Infrared Spectroscopy (FTIR), Atomic Force Microscopy (AFM), X-Ray Diffraction (XRD), and other techniques. The impact of an interlayer of Hexamethyldisilazane (HMDS) between the metal and the pentacene, as well as the substrate and substrate temperature, was studied. From this study it was possible to dismiss the association of one of the carbon chemical species in pentacene to the bonding to Au or TaN. For both substrates, when grown at 55°C the pentacene formed large aggregates and did not cover the whole surface. The roughness of these films was of the order of the film thickness. The morphology of the pentacene films was very dependant of the substrate. On Au the pentacene grew in a dendritic mode, while on TaN nucleated around points scattered on the surface. In contrast to TaN, the HMDS did not stick on gold; however, the treatment affected the pentacene growth by changing the hydrophobic nature of the surface. The effect on the morphology was subtle but present. When the substrate was treated with HMDS the pentacene grains showed more texture. In contrast to the thin pentacene/Au films, the thin pentacene/HMDS/Au films did not show the XRD peaks associated to the (001) spacing. This effect could be explained by considering that the pentacene was induced to grow in a preferential way that prevented the detection of those planes with the 2θ XRD mode.

The whole experimental work was done at The University of Texas at Dallas, within the Material Science Group of the Erik Johsson School of Engineering and Computer Science.

Chapter 1. Introduction

The development of flexible displays that could be rolled on a pen, as well as light electronic devices stuck on clothes, are currently under development in the electronic industry. This research has conveyed to the implementation of new materials. Organics such as pentacene have become the materials of choice because of its high charge mobility. The chemical reaction in the Pentacene ($C_{22}H_{14}$)-Gold (Au) interface has been studied previously. It is desirable to substitute Gold (Au) by Tantalum Nitride (TaN) which is less expensive in an Organic Thin Film Transistor (OTFT).

1.1. Organic Thin Film Transistors

The Field Effect Transistor (FET) is a unipolar device because the generated current is produced by either electrons or holes. In the n-channel FET the current is due to the electrons and in the p-channel the current is due to the holes. The FET is controlled by a voltage between the gate and source. There are two types of FETs; JFET (junction field-effect transistor) and MOSFET (metal oxide-semiconductor field effect transistor).[1] The MOSFET device is formed by a gate (G), drain (D), source (S) and channel.

The operation of the OTFT have been described by several authors.[2,3, 4] A schematic description is shown in Figure 1.1. The components of a field effect transistor (organic or inorganic) are:

- A thin film semiconductor layer which is separated from a gate electrode by the insulating dielectric gate.

- The source and drain electrodes separated by a distance L (channel length) that are in contact with the semiconductor layer.

Figure 1.1   Schematic representation of an OTFT. The electrodes (the source and the drain) are made from a metal, typically Au. Pentacene is becoming the organic "semiconductor" of choice. SiO_2 is commonly employed for the insulating layer.

For an efficient transport of charge through the channel requires a continuous and ordered semiconductor film. The pentacene is grown through vapor deposition, technique that requires low molecular weight to form polycrystalline films with good connectivity between the grains. This semiconductor layer is the subject of the study of this thesis.

1.2. Pentacene as semiconductor

After an extensive search for an appropriate organic semiconductor for field effect transistors, pentacene ($C_{22}H_{14}$) have demonstrated to be the most attractive. Pentacene has been used as a moderate hole transport materia. Highly purified pentacene thin films have exhibited hole mobilities from 1.4 to 0.25 cm^2/V s. [5,6,7] Pentacene films with good morphology and molecular order can be obtained by evaporation on suitably treated dielectric.[8,9,10,11] Organic conductors are classified as polymers and oligomers. The polymers by themselves are not conductive but could reach good conductivities by doping. Pentacene has been classified as an oligomers. As an organic material, its crystal structure is not formed by periodic array of atoms, but by weakly bonded molecules. In organic semiconductors, the conductivity is determined by intermolecular transport. In contrast to polymers, conductivity is between ordered crystal structures. Others molecular conductors that have been studied are anthracene and perylene.[2,12]

The pentacene is a polycyclic aromatic hydrocarbon (PAH) and is composed by five planar benzene rings. The stoichiometry of the molecule is $C_{22}H_{14}$. The orbitals are localized. Three of the four valence electrons of the carbon atom form sp^2 hybrid orbitals that are employed to bond to three neighboring C atoms.[12] The angle between them is 120^0 and σ bonds are generated. The forth electron is in a delocalized p_z orbital perpendicular to the sp^2 hybrid orbital overlapping with neighboring atoms to form π bonds. This π system is responsible for the intermolecular conduction in these materials.[5]
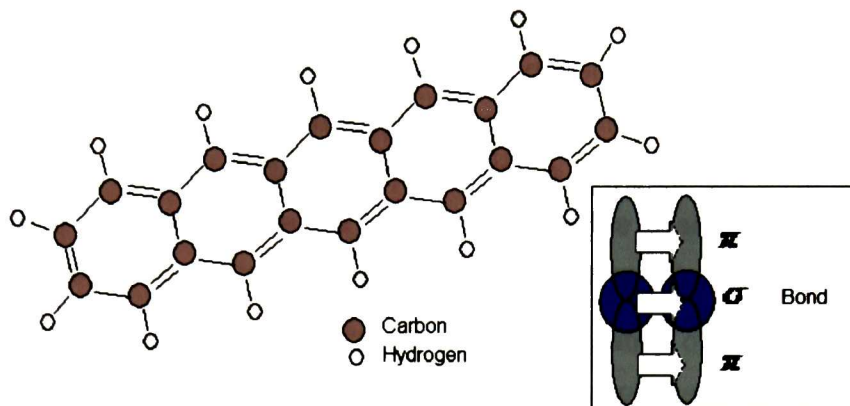
Figure 1.2   Pentacene molecule.

Pentacene crystallizes in layered structure. The arrangement of the flat pentacene molecules on top of each other is defined as the (001) periodicity. For the case of pentacene deposited on SiO_2, values for d(001) of 14.1, 14.4, 15.0 and 15.5 Å were reported.[5] Single crystals commonly adopt the shortest d(001) spacing of 14.1 Å. The growth of different polymorphs depends strongly on the substrate temperature and the film thickness. The most stable structures correspond to 14.1 and 14.4 Å. The 14.4 and 15.4 Å polymorphs appear to be induced by the substrate.[13] The 15 and 15.4 Å structures are less stable and can be changed into 14.1 and 14.4 Å respectively by applying heat by exposure to solvents.[5]

The pentacene density is 1.37 g/cm^3 and is sensitive to light and oxygen.[5,14] Multiple peaks present could be due to several orientations and impurities in the thin film. Films grown at higher temperature show better crystalline structure, and exhibit crystal sizes up to 1μm.[5] During the crystal growth, pentacene is sensitive to oxidation and hydrogenation resulting in single crystals of dyhidropentacene and pentacenequinone.

1.3.   Organic-metal interaction

Part of the objective of this work is to describe the interaction between pentacene with two different metals (Au and TaN). One of them (pentacene/Au) has been already studied. Metal-Organic and Organic–Organic interfaces for small molecule and polymer devices have been studied since the last decade.[15,16,17,18] The metal-organic contacts

generally did not follow the Schottky-Mott model and exhibited large dipole barriers.[15,16,19,20] The metal-organic interface generated additional dipoles. This interfacial dipole is seen as a potential shift across the dipole layer.[15] This shift results in a change in the work function.[21,22] It has been shown that the film morphology (organic material) affects the device mobility.[23,24] In the case of pentacene, a high degree of order is necessary to achieve good transport properties.[8]

The organic-metal interface is very important to the operation of the OTFT. It requires an ohmic contact with low resistance. This allows good carrier injection from the contact into the semiconductor. Historically, Au has been used to fabricate OTFT constructed with pentacene since it has been used as contact material for the source and drain electrodes. There are already several studies of this interaction.[25] When pentacene is deposited on Au(111) surfaces the molecules lay flat and are oriented parallel to each other. The dipole in this case, as measured with Ultraviolet Photoemission, was 0.95eV. The different interface dipoles are related to the different orientations of the pentacene molecules due to different pentacene substrate interaction.[26] Due to the organic-metal interaction, the highest occupied molecular orbital (HOMO) energy level of pentacene is approximately aligned to the Au Fermi Level,[27,28] so Au is an efficient charge injecting electrode in the pentacene films transistors.

The Au usually does not stick on the majority of the materials. The use of Cr as interlayer is an option, but Cr as interlayer affects the OTFT behavior by reducing the contact resistance due to the Cr oxidation[29]. TaN does not need an additional interlayer to be deposited on different materials and its work function is ~4.8 eV, close to that for Au.[30] This material becomes a good choice to substitute Au as contact electrode. There are not reports in the literature on pentacene/TaN. In this thesis are presented a series of studies on the TaN/pentacene system.

1.4. Hexamethyldisilazane (HMDS) treatment

Besides metal-semiconductor interface, the pentacene-dielectric interface is critical for good charge transport in an OTFT.[31] Recent studies have been focused on the surface

modification of dielectrics such as SiO$_2$ using Hexamethyldisilazane, HN[Si(CH$_3$)$_3$]$_2$(HMDS)[32,33] and Octadecyltricosane, CH3-(CH$_2$)$_{17}$-SiCl$_3$ (ODTS).[34,35,36] Both employed to protect the SiO$_2$ surface. The substrate modification with HMDS results in OTFT current improving. This effect was attributed to a reduction in the density of interfacial charge trappings states.[32,37] Since the HMDS treatment is performed after the deposition of the electrodes (see Figure 1.1), it was of interest to find out the effect of HMDS on the electrode-semiconductor interface.

A molecule of HMDS is shown in the Figure 1.3. HMDS treatments have been shown interesting properties. This is attributed to the highly hydrophobic character of the molecule, originated from the large amount of CH3 species within the film. HMDS treatments also facilitates the adsorption of organic compounds.[38,39] Although the Pentacene/HMDS/SiO$_2$ system has been studied[37] (nucleation of pentacene on SiO$_2$ modified by HMDS), there is not enough information about the pentacene/Au/HMDS or the pentacene/HMDS /TaN systems.
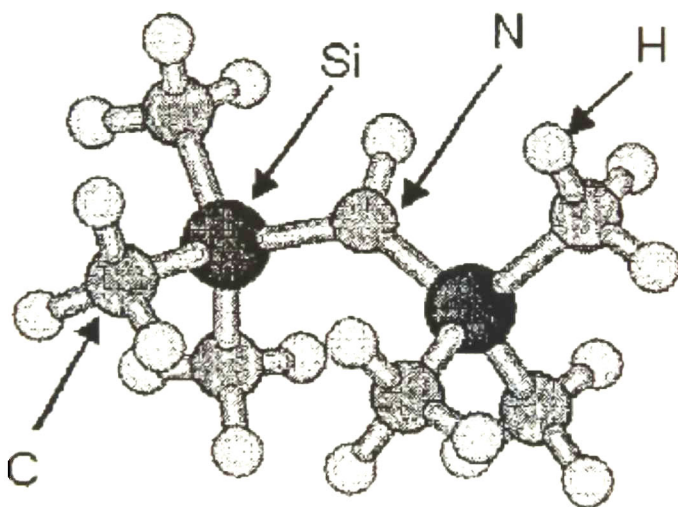
Figure 1.3   Schematic scheme of the HMDS Molecule

1.5.   Objectives

The main objective of the present work was to compare the chemical and physical structure of pentacene films grown on Au and TaN surfaces and HMDS-treated Au and TaN surfaces.

The specific objectives were:

- To prepare Au and TaN substrate for the growth of pentacene films.

- To deposit pentacene films of different thickness on Au and on TaN, with and without a HMDS as interlayer (at RT and 55°C).

- To perform XPS and FTIR analysis to investigate the resulting chemical structure.

- To perform AFM studies to obtain the morphology of the different pentacene films.

- To perform XRD experiments to obtain the microstructure of the pentacene films.

- To determine the effect of the substrate, substrate temperature, and the HMDS interlayer on the pentacene film properties.

References

[1]   Dorf/Svoboda. Electric Circuits, analysis and design introduction 3rd.edition. Edit. Alfaomega

[2]   Chistopher R. Newman, C. Daniel Frisbie, Demetrio A. da Silva Filho, Jean-Luc Bredas, Paul C. Ewbank and Kent R. Mann. Introduction to Organic Thin films transistors and design of n-channel Organic semiconductors. Chem /matter, Rev. june 2004.

[3]   Jana Zaumseil and Henning Sirringhaus. Electron and Ambipolar Transport in Organic Field Effect Transitors. Chem. Rev. 2007, 107, 1296-1323.

[4]   C.D. Dimitrakopoulos, S. Purushothaman, J. Kymissis,A. Callegari, J.M. Shaw, Science 283 (5403) (1999) 822.

[5]   Chistine Corine Matteus. PHD thesis; polymorphism and electronic properties of pentacene. Presented on July 5 2002.

[6]   J. H. Schon, C. Kloc, R.A. Laudise, and B. Batlogg, Phys. Rev. B 58 12952(1998)

[7]   X.L. Chen, A. J. Lovinger, Z. Bao, and j. Spjeta, Chem. Mater 13, 1341 (2001)

[8]   C.D. Dimitrakopoulos, S. Purushothaman, J. Kymissis,A. Callegari, J.M. Shaw, Science 283 (5403) (1999) 822.

9   H. Klauk, M. Halik, U. Zscheieschang, G. Schmid, W. Radlik, J. Appl. Phys. 92 (9) (2002) 5259.

10   T.W. Kelley, L.D. Boardman, T.D. Dunbar, D.V. Muyres,M.J. Pellerite, T.P. Smith, J. Phys. Chem. B 2003 (107) (2003) 5877

11   R. Ruiz, D. Choudhary, B. Nickel, T. Toccoli, K.C. Chang, A.C. Mayer, P. Clancy, J.M. Blakely, R.L. Headrick, S. Iannotta, G.G. Malliaras, Chem. Mater. 16 (2004) 4497.

12   C. Kittel, Introduction to Solid State Physics, 6th Edition (John Wiley , 1986)

13   Oana D. Jurchescu, Jacob Baas and Thomas T. M. Palstra. Applied physics letters 87, 052102 (2005).

14   Lawrence F. Drummy, Paul, K. Mista and David C. Martin. Mat Res. Soc. Sym Proc Vol. 734 Materials research society 2003.

15   H.Ishii,KSugiyama,E.Ito,K.Seki, Adv. Mater (1999) 605.

16   A.Kahn, N. Koch, W. Gao, J. Polym. Sci. Part B: Polym. Phys. 41 (2003) 2529

17   W.R. Salaneck, K. Seki, A. Kahn, J.J. Pireaux (Eds), conjugated Polymer and Molecular Interfaces: Science and Technology for Photovoltaic and Optoelectronic Aplications, Marcel Dekker, New York 2002.

18   Y. Shen, A.R. Hosseini,M.H. Wong, G.G. Malliaras, Chem. Phys. Chem 5 (2004).

19   H. Ishii, K. Seki, IEEE Trans. Electron Dev. 44(8)(1997) 1295.

20   I.G. Hill, A. Kahn, Appl Phys Lett 73 (5) (1998) 662

21   D. P. Woodruff, T.A. Delchar, Modern Techniques of Surface Science,Cambridge University Press, Cambridge 1986.

22   J. Hoelzel, F. K. Schulte, H. Wagner, Solid State Surface Physics,Springer, Berlin 1979.

23   Neil J. Watkins, Serkan Zorba, Li Yan And Yongli Gao. Materials Research Society, Vo. 708 2002.

24   F. Amy, C. Chan, A. Kahn. Organics Electronics 6(2005) 85-91

25   Yen-Yi Lin, David J. Gundlach, Shelby F. Nelson and Thomas N. Jackson, IEEE Transactions on Electron Devices, Vol. 44, No. 8, August 1997.

26   P.G. Shroeder, C. B. France, J. B. Park, and B. A. Parkinson. Journal applied physics, vol. 91, No. 5.

27   V. Bulovic, M. A. Baldo, and S. R. Forrest, in *Organic Electronic Materials*, Vol. 41, edited by R. Farchioni and G. Grosso(Springer, Berlin, 2001)

28   Mat. Res. Soc. Symp. Proc. Vol. 708 © 2002 Materials Research Society

29   Sung Hwan Kim, Hye Young Choi, Jin Jang, Effect of source/drain undercut on the performance of pentacene thin-film transistors on plastic, *Applied Physics Letters*, 4514-4516, 2004.

30 Y. H. Kim, C. H. Lee, T. S. Jeon, W. P. Bai, C.H. Choi, S. J. Lee, L. Xinjian, R. Clarks, D. Roberts and D. L. Kwong. High Quality CVD TaN gate electrode for sub-100nm MOS devices.7803-7050,2001 IEEE.

31 A. Dodabalapur, L. Torsi, and H. E. Katz, Science **268**, 270 _1995_.

32 I. Yagi, K. Tsukagoshi, and Y. Aoyagi, Appl. Phys. Lett. **86**, 103502_2005_.

33 H. Yang, T. J. Shin, M. M. Ling, K. Cho, C. Y. Ryu, and Z. Bao, J. Am. Chem. Soc. **127**, 11542 2005_.

34 M. Shtein, J. Mapel, J. B. Benziger, and S. R. Forrest, Appl. Phys. Lett. **81**, 268 _2002_.

35 D. Knipp, R. A. Street, A. Völkel, and J. Ho, J. Appl. Phys. **93**, 347 _2003_.

36 10H. Klauk, M. Halik, U. Zschieschang, G. Schmid, W. Radlik, and W. Weber, J. Appl. Phys. **92**, 5259 2002.

37 Aravind S. Killampalli and J. R. Engstrom. Applied Physics Letters 88, 143125 (2006).

38 Nogueira S. Caracterização de filmes obtidos a partir da deposição por plasma de hexametildissilazana. [Dissertação de Mestrado]. EPUSP; 2000.

39 Nascimento Filho AP. *Produção de novos filmes para detecção de poluentes*. [Dissertação de Mestrado]. EPUSP; 2002.

Chapter 2. Experimental Techniques

2.1. Cleaning Process

Cleaning is an important part of the semiconductor chip manufacture. At least 50% of yield losses in integrated circuits are due to the micro-contamination.[1] The cleaning of the substrates is a fundamental step in thin film growth and in their characterization.

2.1.1. Wet-Chemical process

The chemicals and the sequence employed in a cleaning process are particular for each surface composition. The Figure 2.1 shows the RCA (Radio Corporation of America) employed in the processes presented in this thesis. Typical cleaning steps employed to clean Si and other wafers in electronics are the following:[2]

- Removal of organic contaminants (piranha, see Section 2.1.1.1).

- Removal of native oxide (HF, see Section 2.1.1.4).

- Particle removal with simultaneous oxide re-growth (SC1, see Section 2.1.1.2).

- Metal removal (SC2, see Section 2.1.1.3).

- Drying (see Section 2.1.2).

After each step a rinse DI water is implemented during at least 1 min. A typical cleaning sequence is piranha, SC1, SC2, and finally HF before the thin film deposition. It is recommended to start with piranha to avoid heavy organic contamination.
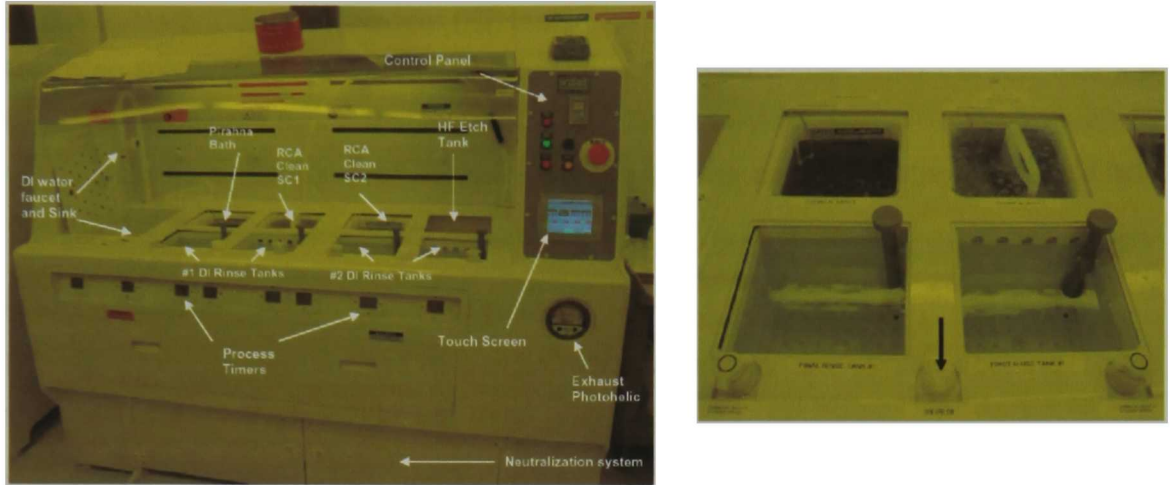
Figure 2.1   RCA hood. Cascade DI Water rinse tanks with controls according to the solutions implemented.

2.1.1.1.   Organic removal (piranha)

This step consists of the removal of organics on the wafer surface. The organic materials make the wafer surface hydrophobic, which prevents further cleaning. The solution employed is H_2SO_4:H_2O_2 6:1 at 85°C for about 10 min.[2]

2.1.1.2.   Particle removal with simultaneous oxide regrowth (SC1)

This step also removes organics, but in particular it removes particles and metals and allow for the growth of a thin oxide film. This oxide passivates the surface by making it hydrophilic (wet with water) and less susceptible to organic and particles contamination. The particles are removed by slow etching form the surface. The etch rate is a function of the type of oxide present. The solution employed is NH_4OH:H_2O_2 :H_2O 1:1:5 at 80°C. A typical etch rate is between 0.09 and 0.4nm/min; the exposure time recommended is 5 min.[2]

2.1.1.3.   Metal Removal (SC2)

The metal removal is usually accomplished using H_2O:HCl:H_2O_2 6:1:1 at 85°C for 10min. It is effective to remove cobalt, copper, iron, leas, magnesium, nickel and sodium as well as aluminum precipitated from the NH_4OH/H_2O_2 solutions.[2].

2.1.1.4. Native Oxide Removal (HF last)

This step removes the oxide on the surface. Its named comes from the fact that the silicon wafer always has a thin layer of oxide. This transform the silicon wafer surface into hydrophobic. The ratio of HF:H_2O is 1:50, and the exposure time is typically one minute.[2]

2.1.2. Semiconductor wafer drying

The water must be remove before it evaporates to avoid leaving residues behind. There are three basic drying mechanisms:

- Physical separation as in centrifugal drying
- Solvent displacement of DI water follower by solvent removal as in vapor drying.
- Evaporation as in hot water.

In the Centrifugal Drying the centrifugal force from spinning wafers at high speed eliminates the major portion of water from the wafer surface. The wafers are centered just off the axis of rotation and rotated at high rpm. The centrifugal force "lock" the wafers in place to prevent tumbling of the wafers and the subsequent particle generation. A spray manifold located at the 1:00 position in the process chamber sprays deionized (DI) water across the wafer surface at a rate of ~1.5 to 2.0 gallons per minute at about 30 psi to remove loosely adhered particles, ionic, and water soluble contaminants.[3]

Figure 2.2 Centrifugal Drying.

2.1.3. UV OZONE treatment

UV/ozone treatment is a well established method for cleaning surfaces and removing organic contamination[4]. This dry surface treatment uses ultra violet light to generate ozone to clean and modify the molecular surface of solids. Low-pressure oxygen and ultra violet (UV) light is used to generate a unique combination of wavelengths that breaks the O_2 bond to form O_3 which is highly reactive. The O_3 bonds with the carbon at the surface, cleaning the surface from contaminants. The process provides enhanced adhesive bonding on plastics, metals and inorganic materials and is also excellent for improving coating process technology. The ozone treatment significantly decreased the water contact on a SiO_2 wafer surface. The sample cleanliness can be maintained at ambient conditions for significantly long time.[5]

Figure 2.3   UV-Ozone cleaning. The equipment employed was Samco UV-Ozone Stripper/Cleaner model UV-1.

2.2.   Deposition techniques

There are several techniques to deposit thin films, and are classified as:

- PVD (Physical Vapor Deposition)

- CVD (Chemical Vapor Deposition)

- Soft Chemistry (Electrodepositing, Sol-Gel, Spray-Pirolisis, Chemical Bath Deposition, etc).

The pentacene is typically grown by PVD. The Physical Vapor Deposition technique consists in the production of a condensable vapor by physical means. Possible methods to generate the vapor are:

- Thermal Evaporation

- Electron Beam

- R.F. Sputtering

2.2.1. Thermal evaporation

In the thermal evaporation PVD the atoms or molecules reach the substrate without collisions with residual gas molecules in the deposition chamber. This requires a vacuum better than 10^{-4} Torr. At this pressure there is still a large amount of undesirable residual gases which could contaminate the film. A higher vacuum is desirable for pentacene deposition.[6] Organics such as pentacene are vaporized by contact to a hot surface that is resistively heated. The heated surface can be in the form of a wire, usually stranded, boat, basket, etc. Typical resistive heater materials are W, Ta, Mo, C, and BN/TiB2 composite ceramics. The deposited material is on an aluminum oxide crucible, which does not react with pentacene, and with a melting point above the process temperature. Some advantages are the following:

- it is possible to reach high deposition rate (0.5 μ/min),

- the low energy atoms (0.1 eV) don't damage the substrate, and

- it is not necessary to heat the substrate.

Some disadvantages are the following:

- there is no control on the stoichiometry in the deposited materials,

- it is difficult to control the thickness,

- the lack of homogeneity in large areas, and

- radiation damage.

To optimize the pentacene semiconductor properties it is recommended a low deposition rate.

2.2.2. Electron beam

Focused high energy electron beams are used to evaporate refractory materials, such as ceramics, glasses, carbon, and refractory metals. Thermo-ionic-emitting filament supplies high electron beam, using high voltages (10–20 kV) to accelerate the electrons, and electric or magnetic field to focus and deflect the beam onto the surface material to be evaporated. Using high-power e-beam sources, the deposition rates are as high as 50 microns per second from sources capable of vaporizing material at rates of up to 10–15 kilograms per hour.

2.3. XPS

The photons interact with the atomic electrons in photon absorption process. For the photoelectric process this is a signature of the photon interaction with the atoms and is the base of the photoemission spectroscopy. Is referred to as UPS when a UV source is implemented to inside on the sample surface and XPS when X-ray is used.

2.3.1. Principles

Based in the photoelectric effect, the X-ray photoemission consist of electrons from core levels absorbing a quantum of energy ($h\omega$) provided by an X-ray and then being ejected from the atom into the vacuum. The electron kinetic energy of those electrons is measured by an electron spectrometer and the data is expressed as counts/seconds as a function of kinetic energy. The kinetic energy (E_K) of the electron is dependent on the photon energy of the x-ray employed and the binding energy (E_B). The relation governing the interaction of a photon with a core level electron is

$$E_B = h\nu - E_K - W,$$

where $h\nu$ is the x-ray photon energy and W is the spectrometer work function. The photoelectron spectrum will reproduce the electronic structure of an element where electrons with binding energy lower than the photon energy will participate in the spectrum. Those electrons which are excited and escape without energy loss contribute to the core level peaks. Other possibility is the ejection of an Auger electron, often

referred as X-AES (X-ray induced Auger electron spectroscopy), which can yield valuable chemical information about an atom.

The depth analysis in XPS depend on the kinetic energy of the electrons under consideration, determining a quantity known as attenuation length (λ) of electrons which is related to the inelastic mean free path (IMFP, that is the probability that an electron travel a distance without lose energy).

The x-ray is generated by electron bombardment of an anode, usually made of Al or Mg. Based in the Bragg relation, the monochromator employs a quartz crystal to produce a narrower X-ray line than the fluorescence line of its anode. The quartz is a convenient material because it is relatively inert, compatible with UHV, and it can be bent into an appropriate shape to focus the beam.

2.3.2. Angle Resolved XPS

The finite mean free path of electrons provides depth information in the order of few nanometers if the electrons are detected at a direction normal to the surface. But if the electrons are detected at shallower angles, the information depth is reduced by an factor equal to the sine of the take off angle. This is the basis of the angle resolved XPS (ARXPS). This technique can be applied to films too thin on the other hand it is non destructive technique which can provide compositional depth profile. The area I_S of a core level photoelectron peak depends on the take-off angle (α) through the following relation

$$\textbf{Equation 1.1} \qquad I_S(\alpha) = C \, X \, A \, \sigma_S \, y_S \, s_S \, \frac{1 - \exp\left(-\dfrac{t_S}{\lambda_S \sin\alpha}\right)}{1 - \exp\left(-\dfrac{a_S}{\lambda_S \sin\alpha}\right)} \overset{\substack{Layers \\ avove\ S}}{\underset{i}{\prod}} \exp\left(-\frac{d_{S,i}}{\lambda_{S,i} \sin\alpha}\right)$$

where a_S is atomic plane spacing of the layer S, s_S the concentration of the specie S in layer S, σ_S the x-ray absorption cross section of the core level, λ_S the attenuation length of the photoelectrons from specie S as they travel through layer S.[7]

2.4. Work Function assessment

Figure 2.4 shows the principle of the measurement of the work function. A sample in vacuum is irradiated with ultraviolet monochromatic light (He I, hv = 21.2eV) and the energy distribution of the emitted electrons (UPS spectrum) is measured. The electrons in the HOMO states show up at an energy given by

$$E_{K,HOMO} = hv + E_{HOMO}$$

where E_{HOMO} is the energy of the electrons in the HOMO states referenced to the vacuum level. Its value is negative. As the diagram illustrates, the cut off comes at an energy given by

$$E_{cut\,off} = E_{HOMO} + WF$$

where WF (work function) is the energy difference between the vacuum level and the HOMO energy. By subtracting these two equations and rearranging we get an expression for the work function in terms of the photon energy and energies that can be extracted from the UPS data:

Equation 1.2 $WF = hv - \left(E_{K,HOMO} - E_{cut\,off}\right)$
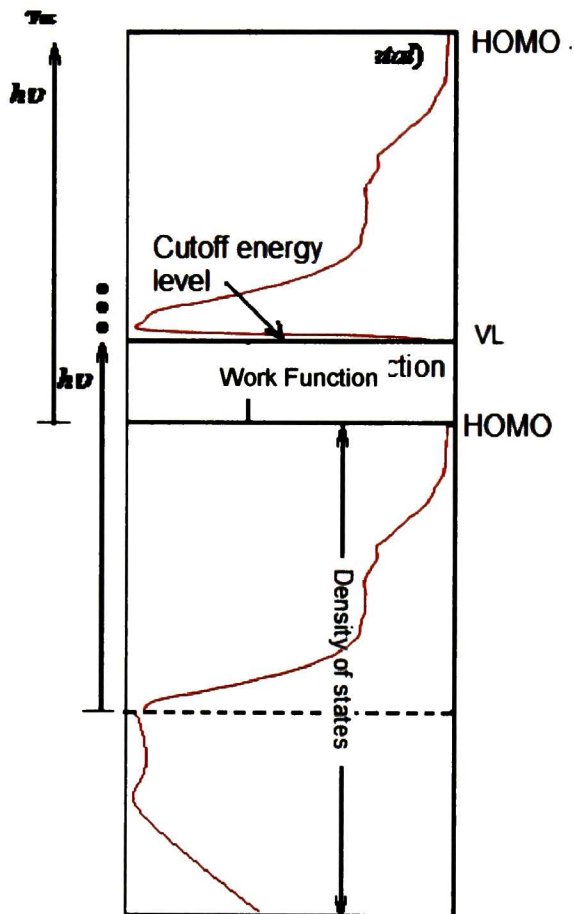
Figure 2.4   Principle of UPS. Organic-Metal energy alignment.

References

[1] Handbook of Semiconductor Wafer Cleaning Technology - Science, Technology, and Applications   Edited by: Kern, W. © 1993 William Andrew Publishing/Noyes.

[2] Roger Robbins and Arnold Duenes. RCA Cleanup Hood Operations. UTD manuals.

[3] Semitool Spin Rinser Dryer 200 Series ST.

[4] D. Guo et al. / Chemical Physics Letters 429 (2006) 124–128

[5] Effect of UV/ozone treatment of the dielectric layer on the device performance of pentacene thin film transistors. Dong Guo *, Shiro Entani, Susumu Ikeda, Koichiro Saiki Chemical Physics Letters 429 (2006).

[6] Handbook of Physical Vapor Deposition (PVD) Processing Mattox, D.M. © 1998 William Andrew Publishing/Notes.

[7]   A. Herrera-Gomez, F.S. Aguirre-Tostado, Y. Sun, R. Contreras-Guerrero, R.M. Wallace, Y. Hisao, and E. Flint. Rapid Communications, Surface and Interface Analysis. In print.

Chapter 3. Experimental Results

Multiple samples and processes were employed in this study. All samples were deposited on silicon wafers. The processing details are described in Section 3.1. The experimental details of all the characterization techniques employed are described in Section 3.2. The Figure 3.8 and Figure 3.9 list all the samples employed and provide a guide for the rest of the sections.

All the processing and characterization described in this thesis was performed within the Materials Science Group of the Electrical Engineering Department of The University of Texas at Dallas.

3.1.   Parameters employed in the sample processing

Some of the principles for the processes are described in Sections 2.1 and 2.2. The specific parameters employed for the processes are listed in this section. The samples were transferred all the time inside a desiccator (alumina was implemented as desiccant) and wrapped with aluminum foil.

3.1.1. RCA cleaning

Table 1.1   Steps in the RCA cleaning.

Step	Process	Container	Solution Temperature (°C)	Time (min)	Stir
1	Pour 6 parts of H_2SO_4 and heat Add one part of H_2O_2 at 65°C.	Glass Beaker on hotplate (5000ml)	85	10	yes
2	"Running" DI water rinse of Si		RT	1	
3	Take 4 parts of H_2O Add 1 part of HF Add 1 part of H_2O_2	Teflon Bucket	RT	1	
4	"Running" DI water rinse of Si		RT	1	
5	Take 5 parts of H_2O Add 1 part of NH_4OH and heat Add 1 part of H_2O_2 at 60°C.	Glass Beaker (5000ml) on hotplate	80	5	yes
6	"Running" DI water rinse of Si		RT	1	
7	Take 6 parts of H_2O Add 1 part of HCl and heat Add 1 part of H_2O_2 at 60°C.	Glass Beaker (5000ml)on hotplate	85	10	yes
8	"Running" DI water rinse		RT	1	
9	HF + H_2O (1:50) ACIDIC	Teflon Bucket	RT	1	

The sample preparation was completed in a cleanroom type 10,000 (i.e., particles/ft^3). The cleaning was critical to the chemical characterization. The RCA cleaning of the p-type Si(001) 4 inches wafers is decribed in Table 1.1

3.1.2. Cr and Au deposition

The deposition of Cr and Au was performed in a focused E-Beam evaporation from Themescal. It was operated manually. The metal depositions were done rotating the chuck where the samples were loaded to get a uniform film thickness. The electron beam needs to be focused on the target material before deposition. The scan rate was manipulated with the current in all deposition.

Silicon wafers of 4" after RCA cleaning were employed as the substrate. To improve the adherence of Au, a Cr layer of about 30Å was deposited prior to the gold deposition. The deposition pressure was 1.32x10^{-9} atm and the deposition rate was manually manipulated. For Cr the deposition rate was between 0 and 1Å/s and the total thickness was 30Å. Two thicknesses of the Au layer were considered: 2000Å (rate lower than 2Å/s) and 500Å (rate lower than 0.7Å/s). The total thickness was measured with a profilometer at six points of the perimeter of the wafer employing the shadows caused by the three clips holding the wafer. All the samples were characterized and measured.
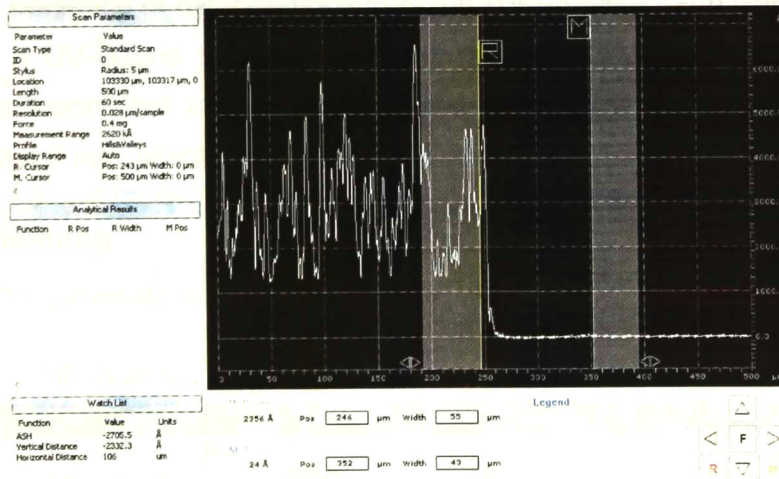
Figure 3.1   Measurement of the Au thickness by the profilometer. The scanning parameters are shown at the top-left and the thickness at the bottom-left.

The Figure 3.1 shows the measurement of the sample nominally of 2000Å. The parameters implemented in the measurement, as well as thickness, are shown at the bottom-left. Although the thickness were within the desired range for all the samples, the apparent roughness was a concern and prompted AFM studies. Some of the AFM images are shown in Section 3.9.

3.1.3. TaN deposition at TI

The TaN substrates provided by Texas Instruments (TI) form the family line S22 in Figure 3.9. The deposition technique employed by TI was CVD with the parameters shown in the Table 1.2. The thickness of the TaN was 500Å deposited on a Si (001) wafer doped at $5x10^{15}$ cm^{-3} previously cleaned by the RCA method.

Table 1.2   Deposition parameters for the TaN films grown at TI.

| Chamber | Deposition conditions | | | |
	Temperature	Gas	Pressure	Other notes
TaN	wf 482C	0.05Torr	Carrier Ar (Taimata) 100sccm	Dilution Ar 470sccm, NH3 200sccm

3.1.4. UV ozone cleaning

The hydrocarbons affect the pentacene deposition. The surface treatment was carried out to prevent presence of hydrocarbons from the environment. The cleaning of the Au was done by a UV-Ozone technique defined in Section 2.1.3. The purpose was to remove contaminants that affect the pentacene and HMDS deposition. The process time chosen was 7 min, which was considering enough to clean the Au surface.

3.1.5. HF cleaning

The HF cleaning parameters are shown on the Table 1.3.[1]

Table 1.3   HF cleaning

	Specifications	Temperature	Etch rate (Å/s)	Exposure time (min)
Acetone	99 - 100% purity	RT		1
HF	Ratio of 1:2; HF:H_2O	60^0C	0.06	1
DI water	No rinse	RT		5 min
N_2	Dry	RT		5 min

3.1.6. SC1 cleaning

The cleaning method for TaN employed was a variation of the SC1 method by Miles Selvidge and Isabel Medina.[2] The parameters are shown in the Table 1.4.

Table 1.4   SC1 cleaning

	Specifications	Temperature	Etch rate (Å/s)	Exposure time (min)
Acetone	99-100% purity	RT		1
SC1	Ratio of 10:1:1; $NH_4OH:H_2O_2:H_2O$	80^{0}C	0.08	0.5
DI water	No stirring	RT		5 min
N_2	Dry	RT		5 min

The exposure time in SC1 cleaning was reduced until a clear brown color was kept by the sample even after exposure to the atmosphere. The samples with longer exposures than 0.5min showed an evolution from brown to gray upon contact with air.

3.1.7. HMDS deposition

This process employed in this study is shown in Table 1.5.[3]

Table 1.5   Y.E.S. Process Recipe. The table below list the recipe used on the vapor prime oven the recipe is the manufactures recommended process.

Dehydration and purging oxygen fro chamber		
	Function	Time
1	Vacuum (10 Torr)	1 min
2	Nitrogen (760 Torr)	3 min
3	Vacuum (10 Torr)	1 min
4	Nitrogen (760 Torr)	3 min
5	Vacuum (10 Torr)	1 min
6	Nitrogen (760 Torr)	3 min
Stage 2: Priming		
	Function	Time
7	Vacuum	2 min
8	HMDS (6 Torr)	5 min
Stage 3: Purging Prime Exhaust		
	Function	Time
9	Vacuum	1 min
10	Nitrogen	2 min
11	Vacuum	2 min
Stage 4: Return to atmosphere		
	Function	Time
12	Nitrogen	3 min
	Total tume	27 min

For reasons shown elsewhere,[3] these steps are called "five cycles."

3.1.8. Pentacene growth

The Pentacene deposition, described in Section 2.2.1, process was done with a Denton Vacuum Evaporator. The deposition rate was controlled with a PID (proportional differential and integral) designed by Srinivas-Gowrisaner from UTD. The design was developed using a programmable logic controller (PLC). The pentacene thickness was monitored by a quartz crystal deposition controller. Pentacene deposition consists on 4 steps:

- rise to soak,
- soak and hold,
- rise to predeposit and
- deposition.

The parameters employed were: rise time to soak 2 min, rise to predeposit 3 min, predeposit time 5 min, predeposit power 8.1% (9 Amperes), soak 6.5 % (5 min), and deposition pressure 2.6 x 10^{-7} Torr. The Denton thermal vacuum evaporator located on the cleanroom was employed. The thickness was monitored by a quartz oscillator and later corroborated using a dektak profilometer. The Figure 3.2 shows an overview of the complete pentacene deposition process. The behavior of a PID controller is described on the Figure 3.3. The PID values were P=100, I=99.9 and D=99.5, which were determined after several depositions to set the deposition rate at 0.5 Å/sec.
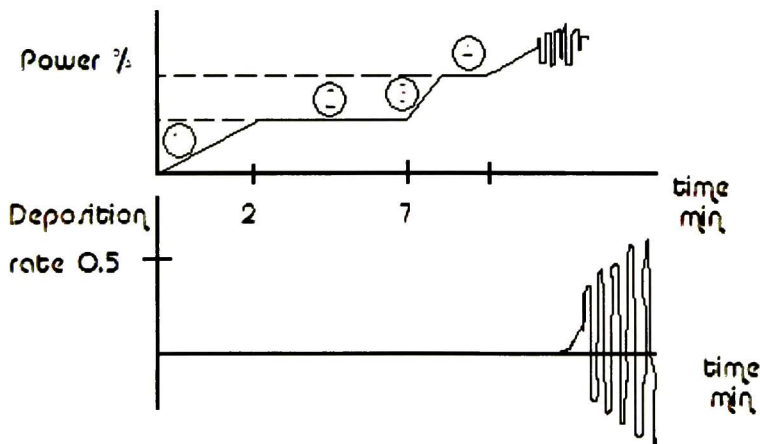
Figure 3.2   Pentacene Deposition. Denton Vacuum evaporator process set up.
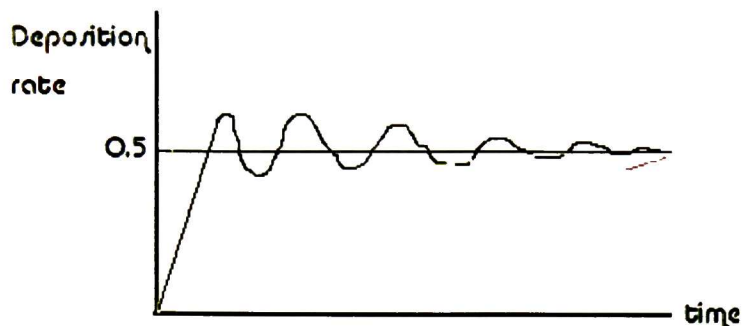
Figure 3.3 Pentacene deposition. PID controller. Where P=100, I= 99.9 and D=99.5.

The Figure 3.4 shows one of the thickness measurements employing profilometry. The pentacene thickness for all samples was measured.
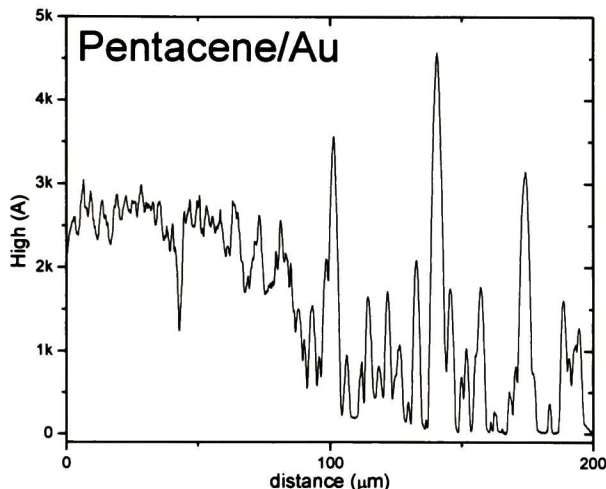
Figure 3.4 Profilometer measurement of a 1500Å (nominal) pentacene film grown on gold (2000Å thick). The profilometer measurements were consistent with the thickness given by the crystal quartz during the deposition.

When the substrate was heated during the pentacene deposition, the temperature of the chamber was maintained at 145°C (it takes 6 hrs to reach that temperature). Under these conditions, the substrate temperature was 55°C, which was the desired value. The pressure in the chamber during pentacene deposition at 55°C was approximately 1.5×10^{-7} Torr. The pressure for the cryo chamber was maintained at 8×10^{-8} Torr. The rest of the parameters varied slightly from those listed above: rise time to soak 2 min,

rise to predeposit 3 min, predeposit time 5 min, predeposit power 9 % (9 Amperes) soak 6.5 % (5 min).

3.2. Parameters employed in the characterization

After the preparation the samples were wrapped up with aluminum foil and keep inside a dessiccator. The characterization techniques employed were XPS, XRD, UPS, FTIR. AFM, and contact angle.

3.2.1. XRD

The X- ray diffraction patterns (XRD) of the pentacene thin films on different substrates were measurements in the A Rigaku Ultima III X-ray Diffractometer system. The x-ray data was obtained in a 2θ mode. The x-ray patterns were fitted using the software AAnalyzer.[4]

3.2.2. Contact angle and surface tension

The equipment Ramé-Hart, Inc., NRL Contact Angle Goniometer, Model 100-00-(115) was used to measure the contact angle. Using 3μL of de-ionized water we place a drop on the surface of each sample. The typical accuracy of a goniometer is ±2°. Figure 3.5 shows the measurement pattern, and how the samples looked with and without HMDS.
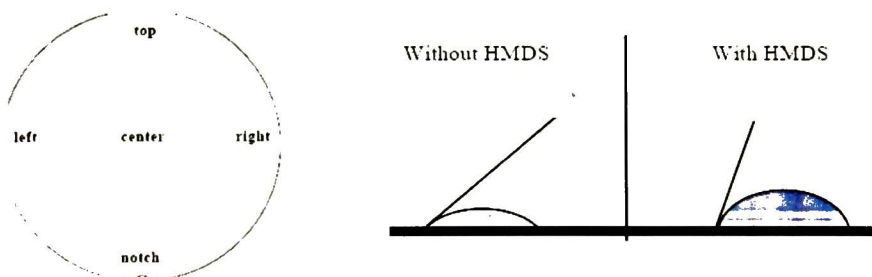
Figure 3.5   Contac Angle Gionometer. (a) Measurement pattern. (b) Surface sample affected by HMDS.

3.2.3. AFM

The atomic force microscopy (AFM) technique provides information about the morphology of the film. The AFM images were obtained from on a Digital Instruments nanoscope system using an ohm silicon cantilever and operating under tapping mode.

The surface roughness average (Ra) and the Roughness mean square (RMS) were determined using the software of the equipment (Nanoscope). The parameters manipulated during the measurements were: scan size, scan rate, samples lines, the integral and the proportional gain and the amplitude set.

3.2.4. UPS

The UPS experiments were done using He I (21.2 eV) line of a discharge lamp UPS spectra acquired with a bias of -5 V to enable the observation of the low energy secondary cutoff. The base pressure was 1x10-8 mbar. After several measurements and comparing with spectra in the literature, it was concluded that the best parameters were pass energy (CAE) 10 eV and dwell 0.5s. The running time was 12 min. The exit slit employed was the number 1 (size of 1x10 mm) and the in-slit was the number 2 (6mm diameter).

3.2.5. XPS

The XPS studies were performed using an ESCA lab system equipped with an Al Kα (1486.7 eV). XPS spectra were collected to 45^0 respects to the sample surface. The software AAnalyzer was employed for the XPS spectra fitting.[5] The XPS spectra were collected at take off angle of 45°. The chamber pressure was at $2x10^{-11}$mbar. The pass energy (CAE) was 10 eV, dwell time 0.2s and the steps were separated by 0.2eV and the number of sweeps depended on the region measured. The running time was about 49 min.

3.2.6. ARXPS

The equipment employed is shown in Figure 3.6.
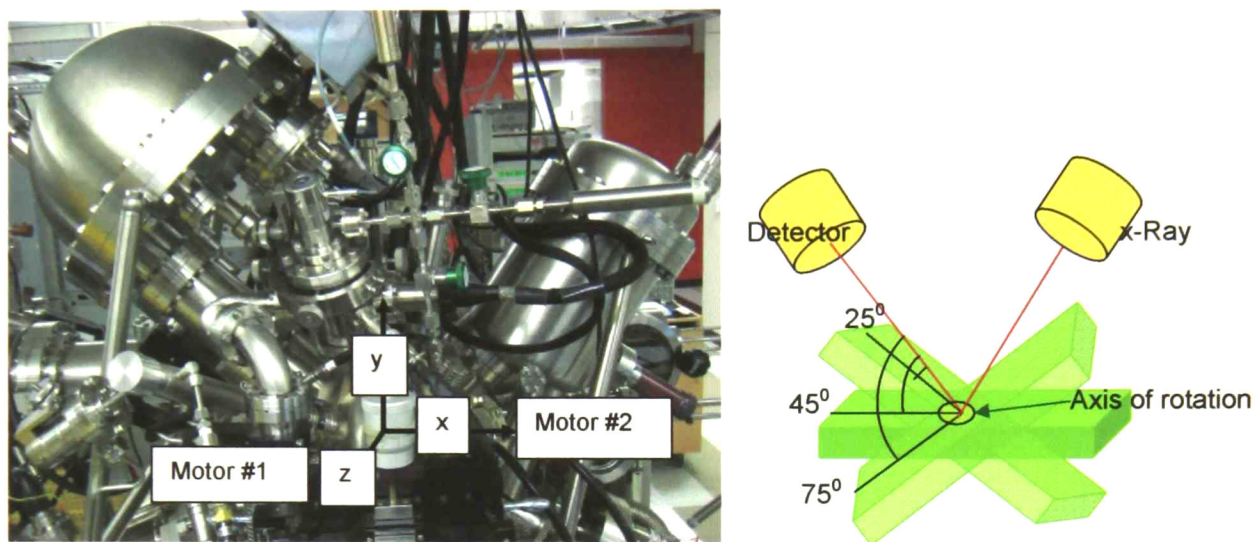
Figure 3.6   Omicron XPS equipment.

The steps in the ARXPS experiments are the following:

- The sample is loaded in the small sample holder. The required slides to position the sample surface at the axis of rotation of the manipulator are added.   The assessment of the thickness of the slides is described in the second step. This could be an iterative process if the height of the sample is too far from the axis of rotation. The positions and size of screws should be of such a size to avoid affecting the measurements.

- The sample is aligned. The sample is positioned in the X-ray source and Detector focal point, adjusting X, Y and Z to maximize the counts. Y is found manually and Z using motor #1. The sample is rotated to 75° and the X position is optimized. The X reading is called X_{75}. Similar steps are followed with the sample at 25°, generating the X_{25} value. The sample is positioned at the X average. XPS data for some core level is obtained at 75° and 25°. The data is fitted using Multipack. The energy shift between the peaks taken at the two angles must be less than 0.03. When $X_{75} < X_{25}$

the sample is below the axis of rotation; when $X_{75} > X_{25}$ the sample is above the axis of rotation.

- The software Cascade was implemented as tool to rotate the sample and get the spectra. To use Cascade instead of manipulating manually the motors it is necessary to allow Cascade to have control over the X-ray source, the EIS and the manipulator (motor 1 and motor 2). Cascade was easy to operate. A diagram describing the operation is shown in Figure 3.7.
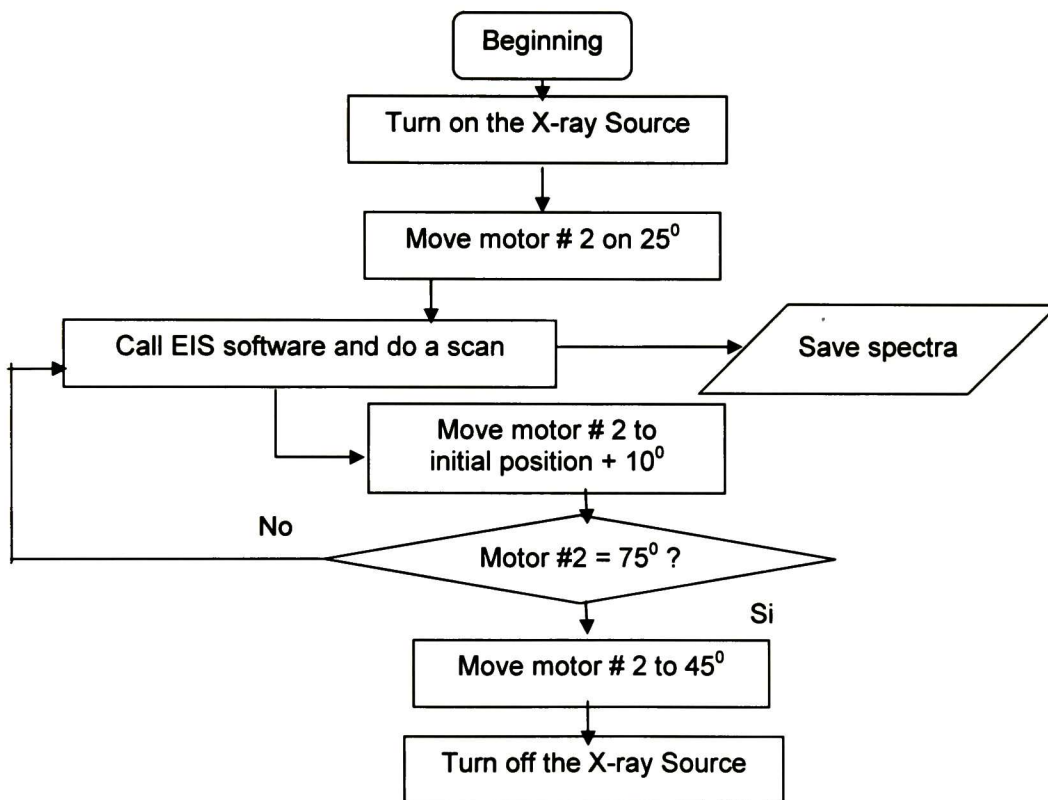
Figure 3.7   Flow diagram for ARXPS data acquisition spectra using the software Cascade.

The XPS spectra were obtained at six different take-off angles respect to the sample surface: 25°, 35°, 45°, 55°, 65° and 75°. The measurement time and the regions were controlled by Cascade. The power employed for the x-ray source was 300 W; the voltage was 15 KV. The work function of the equipment and the calibration was

determined every month. The reason to use CAE with a value of 10 eV was to maximize the resolution avoiding too much exposure and pentacene damage. All this parameters are in the window of the EIS software of this equipment.
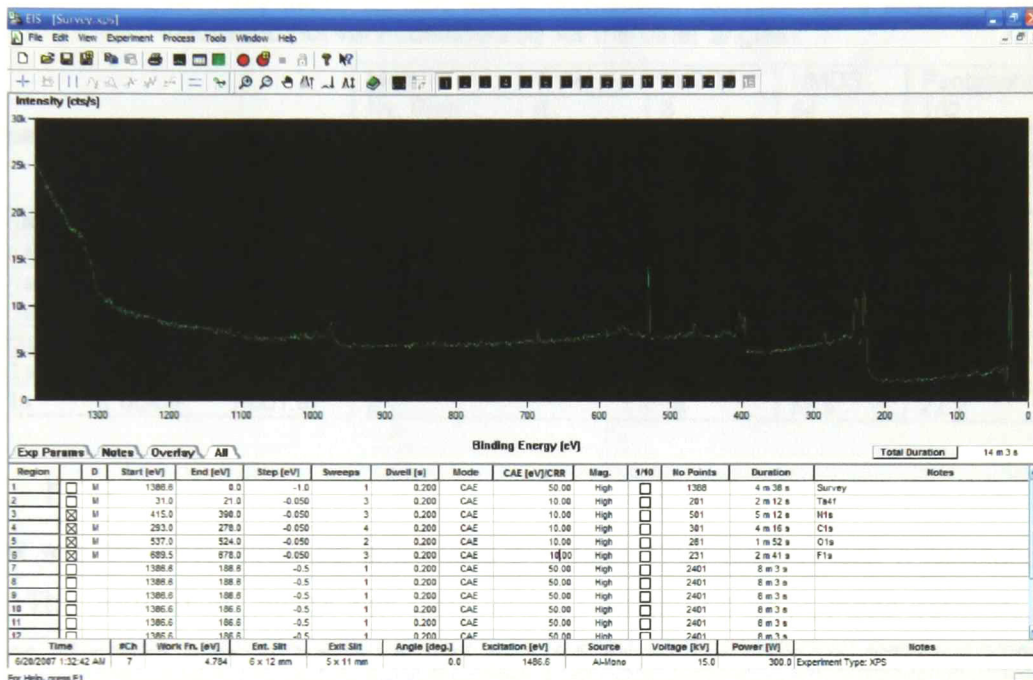
The pentacene/Au ARXPS data taking time was 22 hours per sample. The spectra were obtained on UHV. The pressure inside the chamber during the ARXPS was 2.6x10^{-11} mbar.

3.2.7. ARXPS data analysis

The order of the magnitude of the thickness of the HMDS was quantitatively assessed with the program XPSGeometry[6] which employs Equation 1.1. The parameters fed to XPSGeometry are shown in Table 1.6.

Table 1.6 Parameters for the different materials employed in the NIST Database software to calculate the effective attenuation lengths, also listed. The EAL was calculated using the Tanuma, Powell, and Penn formula. Other information employed was that the photon source was Al *Kα* x-rays. A 45° x-ray incidence and 45° photoelectron detection were assumed (the values did not vary considerably for the other angles).

Peak Info			Material->	TaN	Ta2O5	HMDS	Pentacene
			Nv. Sum	8	8	54	102
			Gap (eV)		4.5'		1.85
			Density (g/cm3)	13.7	8.2	0.77	1.37
Peak	BE (eV)	KE (eV)	Asymetry β	EAL (Å)	EAL (Å)	EAL (Å)	EAL (Å)
Ta4f	23.2	1463.5	1.6	16.5	25.3	37.57	36.473
C1s		1202.1	2			31.9	30.990
O1s		955.5	2		18.8	26.4	27.434
Si2p		1387.4	1.03			35.9	37.340
N1s	396.6	1090.1	2	11.5		29.4	28.576
F1s	684.9	801.8	2		16	34.9	22.2

3.2.8. FTIR

The IR spectra were obtained employing a Nicolet 4700 system with a resolution of 4cm^{-1}. The germanium crystal was used as the background an all measurements. The number of scans was 100 per sample and 64 scans for background (the software employed for the analysis, Omnic V7.2a, allows for the use of different number of scan for the sample and the background, and corrects for this difference). The spectra were acquired in the ATR mode. The position of de peaks (maximum) was determined using the software of the equipment. The assignment of the pentacene peaks was done according to the Spectral Database for Organic Compounds (SDBS) of pentacene.[8]

3.2.9. Profilometry

The equipment employed was a DEKTAB from Digital Instruments. The force implemented in the profilometer measurements was 0.1 mg (to avoid the pentacene film damage). The mode of the profile measurement was hill and valleys. The resolution used was of 0.033 um/sample, and a length of 500μm.

3.3. Description of the samples

The processes and characterizations performed on the different samples are diagrammatically described in Figure 3.8 and Figure 3.9.

The Structure of Pentacene Films Grown on Au and TaN Substrates

Si (001) with RCA cleaning → 30Å Cr → 500Å Au (s11) → AFM, XPS FTIR, CA → UV-Ozone (s111) → **XPS, FTIR, CA**

XPS, FTIR, CA → (25 c) HMDS (s1111) → Pentacene → 3nm(s11111) → XRD
3nm(s11111) → 25nm(s11112) → XRD
→ 50 nm(s11113) → XRD
→ 150 nm(s11114) → XRD XPS

AFM,FTIR,Contact angle
(5 c) HMDS (s1112) → XPS
(15 c) HMDS (s1113) → XPS → Pentacene → 30 nm(s11115) → XPS UPS → XPS

(5)HMDS (s1114) → Pentacene Heating → 3nm(s11145) → XPS UPS
→ 12nm(s11146) → XPS
→ 27nm(s11147) → XPS
→ 30 nm(s11148) → XPS FTIR
XPS FTIR AFM

2000Å Au (s12) → AFM, UPS → Pentacene → 3nm(s121) → ARXPS UPS
→ 150nm(s123) → UPS
Pentacene Heating → 3nm (s122) → XPS, UPS

Pentacene → 3nm(s1121) → XPS FTIR AFM
→ 25nm(s1122) → XPS FTIR AFM XRD
→ 50nm(s1123) → XPS FTIR AFM XRD
→ 150nm(s1124) → XPS FTIR AFM XRD → XRD → Sputtering → 50 Å(s11221) → XPS
Sputtering → 25 Å (s112211) → **Sputtering** → XPS
Sputtering → 3 Å (s1122111) → **XPS**

Pentacene → 3nm(s131) → XPS
→ 12nm(s132) → XPS
→ 27nm(s133) → XPS
Pentacene Heating → 30nm(s134) → XPS FTIR AFM
→ 37.5nm(s125) → XPS FTIR AFM

Figure 3.8 Processing and characterization for the samples grown on gold.

31

The Structure of Pentacene Films Grown on Au and TaN Substrates

500Å TaN fromTi (S21)

Si (001) with RCA cleaning

AFM, XPS, FTIR

HF (S211)

XPS, AFM

SC1 (S212)

XPS

(25 C) HMDS(S2111)

(25 C) HMDS(S2112)

(25 C) HMDS(S2113)

XPS

XPS

AFM,FTIR,Contact angle (3.6)

Pentacene

3nm(S21111)   XRD

25 nm(S21112)   XRD

37.5 nm(S21113)   XRD

50 nm(S21114)   XRD

150 nm(S21115)   XRD

Pentacene Heating

30nm (S2114)   ARXPS FTIR, AFM

Pentacene

3nm(S2115)   XPS, FTIR, AFM XRD

25 nm(S2116)   XPS, FTIR, AFM XRD

50 nm(S2117)   XPS, FTIR, AFM

37.5 nm(S2118)   XRD

150 nm(S2119)   XPS, FTIR, AFM XRD

Pentacene Heating

30nm (S2116)   ARXPS FTIR,

Sputtering   50 Å (S21117)   XPS

Sputtering   25 Å (S211111)   XPS

Sputtering   3 Å (S2111111)   XPS

Figure 3.9   Processing and characterization of the samples grown in TaN.

32

3.4.   The Gold (Au) substrate

3.4.1.   The effect of the deposition rate and thickness on the Au film morphology

Because of the apparent roughness shown in the profilometer measurements section 3.2.9, it was decided to study the surface morphology with AFM. The images obtained are shown in the Figure 3.11 for the sample S11 and Figure 3.10 for the sample S12. Parameters implemented in the measurement are scan size of 1x1μm (sample S111) and 2x2μm. The scan rate was done at 1 Hz, 512 samples lines, integral gain 0.5 and proportional gain 0.7. The amplitude set was chosen at 379 mV.

a)

b)
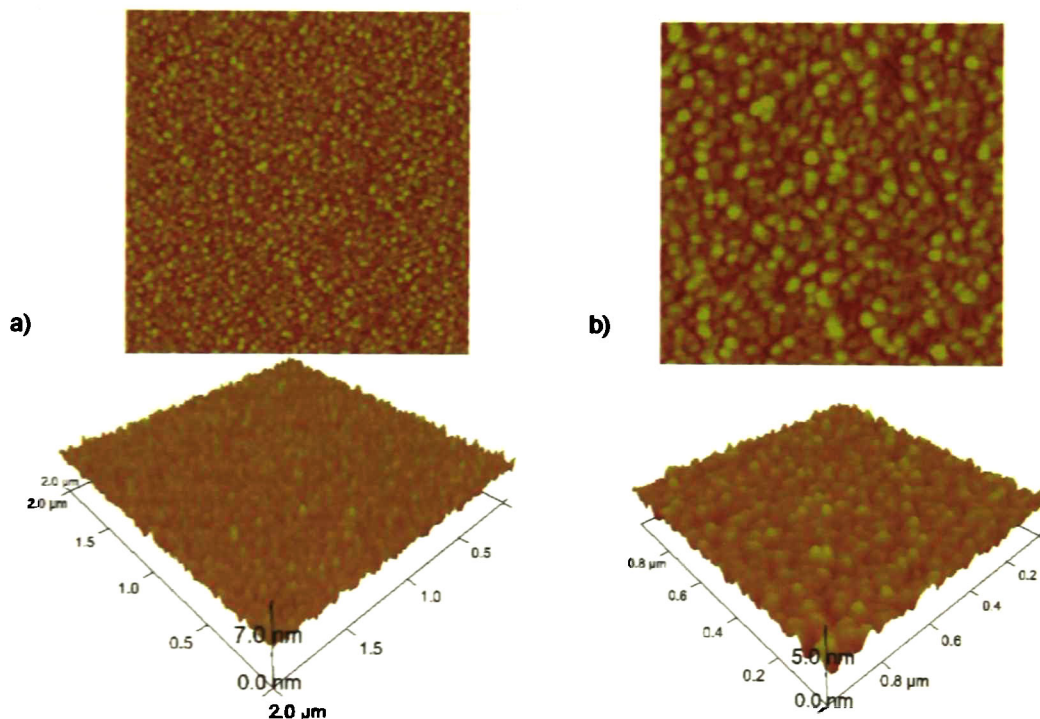
Figure 3.10   Sample S11 (see Figure 3.8). AFM tapping mode of a sample of a thin film of Au deposited on a Si wafer. Scan size: a) 2x2μm and b) 1x1μm.

Figure 3.11   AFM tapping mode of a sample of a thin film of Au deposited on a Si wafer. Sample S12 (see Figure 3.8). Scan size: 2x2μm

The roughness is shown in Table 3.1.

Table 3.1   The RMS values for the correspondent sample are:

Sample Label	RMS (nm)	Roughness average (nm)
S12	1.7	1.4
S11	0.5	0.4

The deposition rate affects directly to the roughness on the surface.

3.4.2.   The effect of the UV ozone on the Au surface chemistry

Au samples before and after UV-Ozone cleaning were analyzed by XPS, FTIR and contact angle to observe the effect of the treatment. The samples employed in this study were S11 and S111 (see Figure 3.8). Both Au samples were loaded in the XPS chamber at the same time.
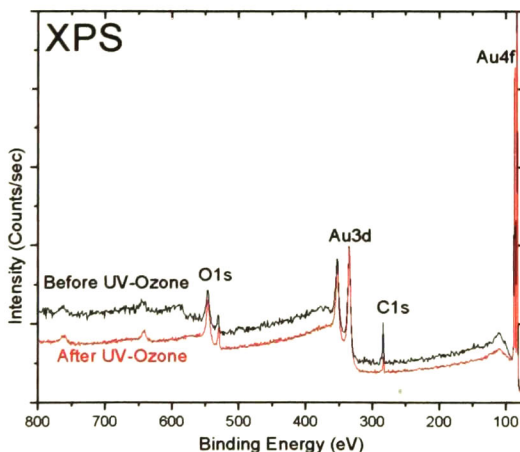
Figure 3.12   XPS spectra for the clean and uncleaned gold surface. The amount of oxygen increased and of carbon decreased with the ozone treatment.

34

The survey spectrum shows that the peaks for carbon (C1s), oxygen (O1s) and gold (Au4f) change upon UV-Ozone cleaning. The spectra of both samples are shown in the Figure 3.12. The Au 4f peak intensity increased after UV-Ozone cleaning due to the removal of the hydrocarbons. On the other hand carbon region C1s decrease and the oxygen region increase after UV-Ozone cleaning. The enhancement of oxygen on the surface after cleaning is due to the UV-Ozone treatment.

The contact angle for both Au samples was measured. The sample with no UV-Ozone treatment showed hydrophobicity (35°), while the sample with treatment got wet.

3.5. The cleaning of the Tantalum Nitride surface

The TaN react easily with the oxygen from the environment to form Ta_2O_5. The treatment implemented to remove this oxide from the surface was standard cleaning 1 (SC1) and HF. XPS measurements were employed to verify the cleaning. Three different samples were compared: TaN- no cleaned, TaN- cleaned by SC1 and TaN- cleaned by HF (samples S21, S211, and S212, as in Figure 3.9). The survey spectrum showed the features for Ta4f, N1s, O1s and F1s.

The XPS spectra fitting provide detailed information about chemical environment and the presence of the Ta_2O_5. The deconvolution of the spectra was similar to other reports in the literature.[9,10] The fitting parameters employed are shown in the Table 1.7.
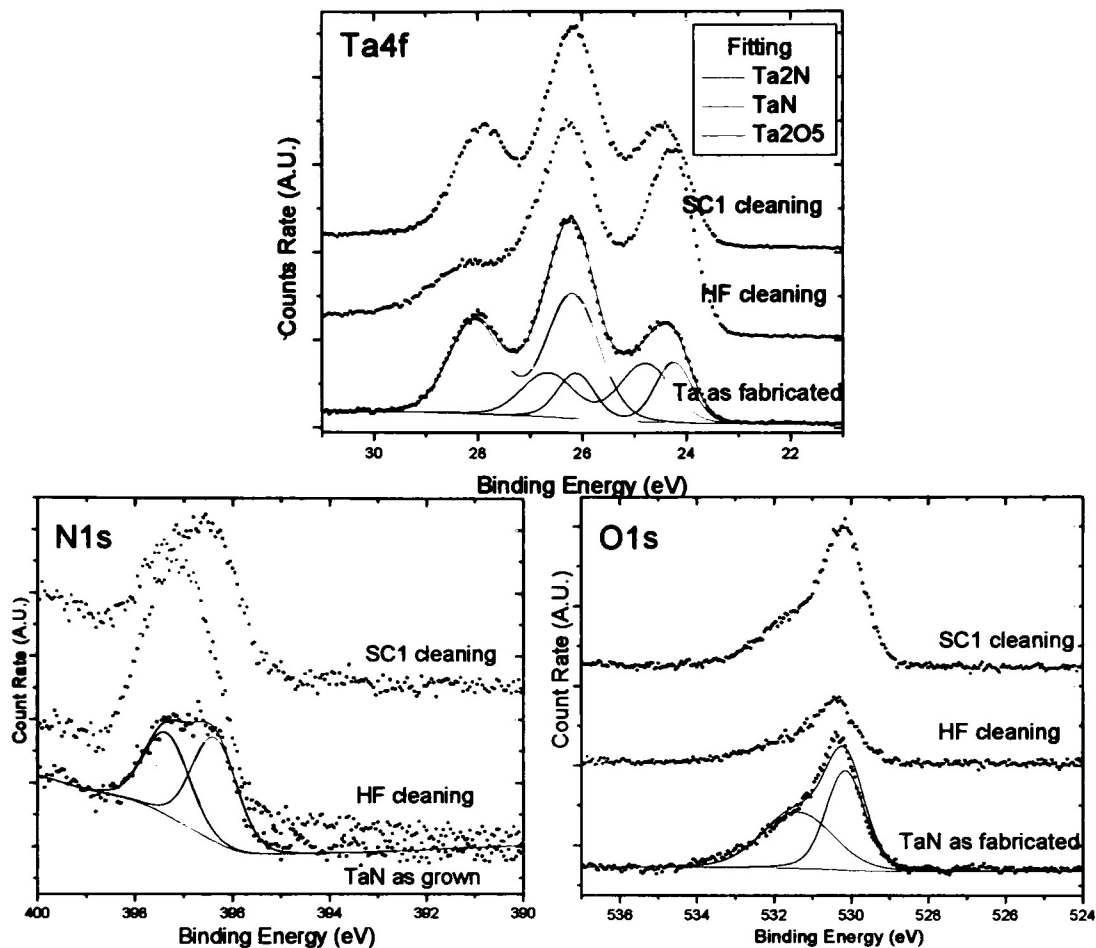
Figure 3.13 XPS Spectra. Comparison of the cleaning (a) Ta4f region clearly HF cleaning shows how Ta_2O_5 is removed selective (b) N1s region nitrogen shows up with the HF treatment, which is consistent with the removal (c) O1s oxygen signal decrease after HF cleaning significantly.

Table 1.7 XPS Spectra. TaN sample parameters spectra fitting.

Ta 4f	Splitting	Ratio	Gaussian	Lorentzian	BE (eV)	Bonding assignment[1][30]
Doublet			0.859		24.65	TaN
	-1.94	0.75	0.665	0.13	24.14	Ta_2N
			1.174		26	Ta_2O_5

The XPS spectra and fits for the different samples are shown on Figure 3.13. The HF treatment removed the Ta_2O_5 and the signal from Ta_2N and TaN increased. The O1s signal also decreased significantly after HF cleaning. On the other hand, SC1 cleaning does not show significant changes comparing to the sample with no treatment in all the regions considered. The HF cleaning introduced fluorine. The amount of fluorine was

reduced (but not removed) by rinsing with water for 5 min. Nevertheless, the conclusion was that the best cleaning treatment was HF.

The surface morphology characterizations with AFM were done before and after the HF treatment (samples S21 and S211 from Figure 3.9) are shown in Figure 3.14. The scan size was $1 \times 1 \mu m$ (scan rate 1.95Hz, amplitude 345 mV) for the sample before the treatment scan size $500 \times 500nm$ (scan rate 0.5 Hz, lines 1024, integral gain 0.5, proportional gain 1, amplitude 360 mV). The untreated TaN surface exhibited grains spread uniformly over the film; the RMS surface roughness was 1.65nm and the average 1.3nm. After cleaning the grains were smeared and the surface was not as uniform. The RMS surface roughness (slightly) increased to 1.9nm and the average to 2.4nm.

500nm

TaN before HF treatment   TaN after HF treatment
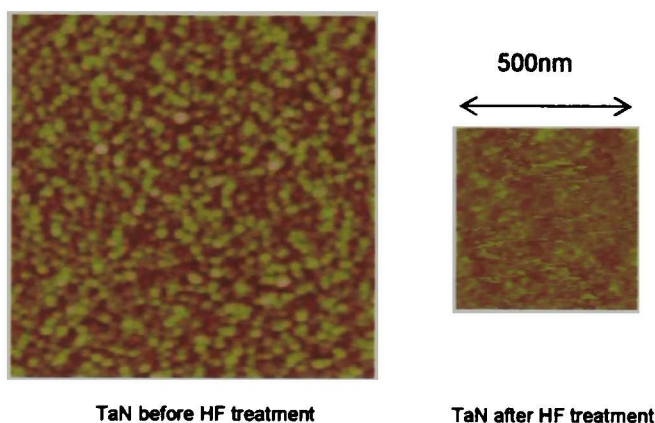
Figure 3.14   AFM tapping mode images of TI TaN samples before and after HF cleaning. The treatment smeared the grains apparent in the untreated sample. The RMS roughness was 1.6nm before cleaning and 1.9 nm after cleaning.

3.6.   HMDS deposition

3.6.1.   Samples

The HMDS treatment is described in Section 3.1.4. Several depositions of HMDS were done and characterized by various techniques such as contact angle, XPS, FTIR and AFM. Before HMDS deposition the Au and TaN surfaces were cleaned (see Sections 0 and 3.1.5). The measurements were compared with samples with no HMDS treatment.

Five cycles of deposition correspond to one monolayer of HMDS on SiO2.[12] The number of cycles implemented and the measurements performed are described on the Table 1.8.

Table 1.8 HMDS Depositions and experiments performed (the sample nomenclature is shown in Figure 3.8 and Figure 3.9).

Sample	Deposition (prime cycles)
Au	0 (S111)
	5 (S1112)
	15 (S1113)
	25 (S1111)
TaN	0 (S211)
	5 (S2111)
	15 (S2112)
	25 (S2113)

3.6.2. Contact angle

The contact angle measurements were done on different points of the samples. The results (see Figure 3.15) show that the hydrophobicity caused by the HMDS deposition stabilized after a few cycles of HMDS growth. The number of HMDS cycles and the contact angle increase on TaN as substrate comparing to the sample without any HMDS treatment. To quantification of the HMDS amount was done through XPS and FTIR.
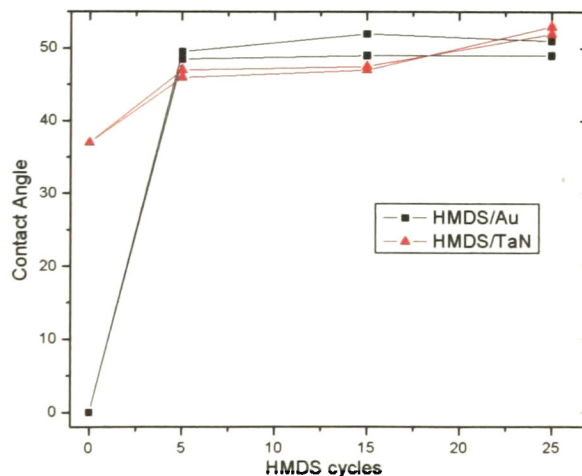
Figure 3.15 Contact Angle measurements for HMDS deposited on Au and TaN with different number of treatments ("cycles", as defined in Section 3.1.4). The contact angle increased with the HMDS treatment.

3.6.3. FTIR

The IR spectra of HMDS commonly shows features corresponding to Si-CH$_3$ (1250-1260 cm^{-1}), Si-CH$_2$-Si (1090-1020 cm^{-1}) and Si-N-Si (900-830 cm^{-1}).[13,14] These regions are shown in the Figure 3.16. The Si-CH$_3$ bond increased notably with HMDS deposition for the TaN substrate. The same behavior was observed for the Si-CH$_2$-S bond, while there was no evidence of Si-N-Si bonds. The IR spectra show that HMDS have a better adhesion for TaN substrate since no changes were observed for the Au substrates.
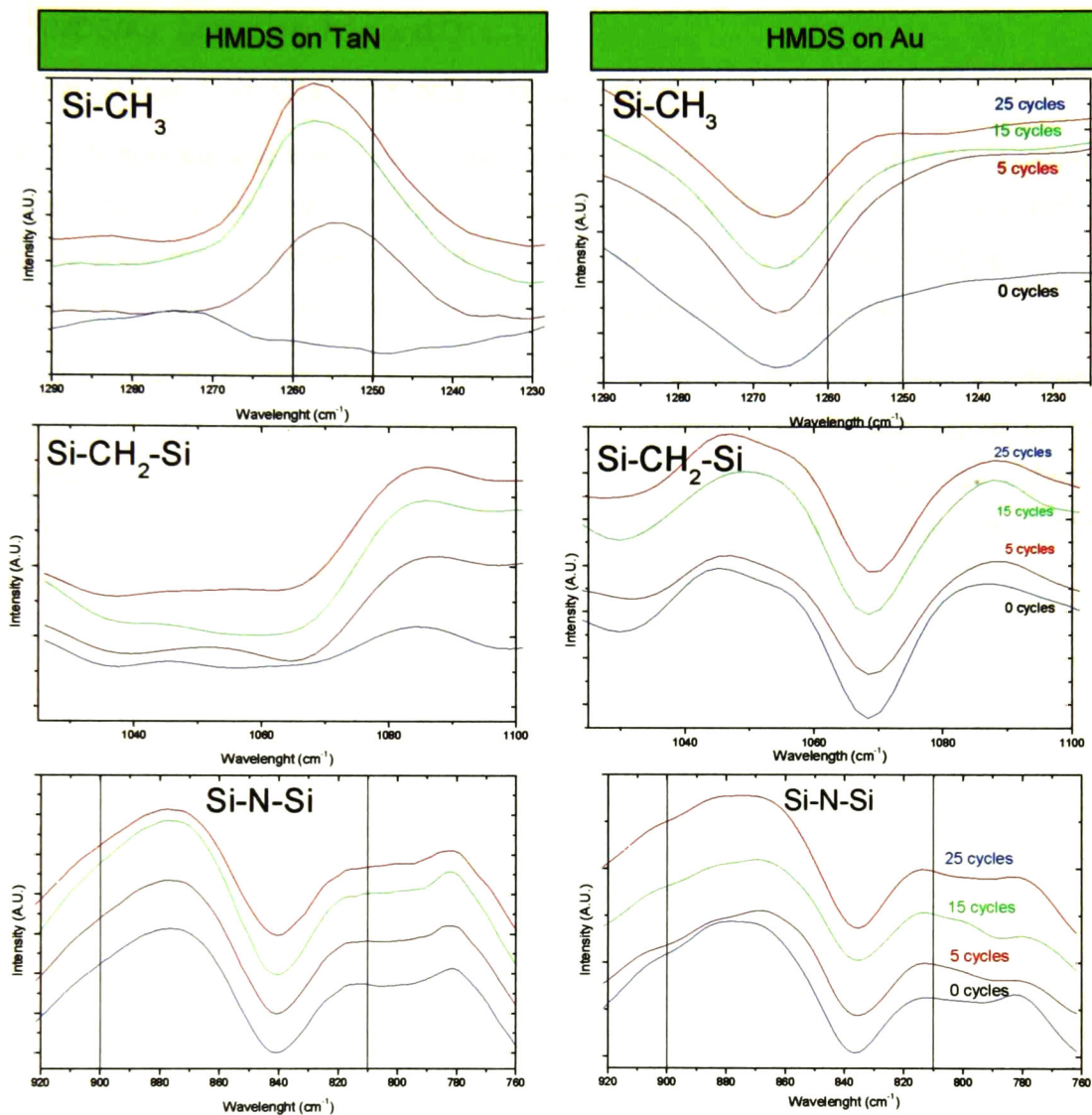
Figure 3.16   The FTIR spectra show the evolution of the HMDS deposition. Comparison of HMDS on TaN (left side) and Au (right side). The signal from the Si-CH₃ and Si-CH₂-Si bonds are clear for the TaN substrates. However, the signal from Si-N-Si was not appreciable. There was no evidence of HMDS deposition on Au substrates. The presence of "negative" peaks is an artifact of the measurement and is possibly due to the small amount of the material.

3.6.4. XPS

XPS provides information about the chemical state of the elements in the surface. The regions measured for each sample were:

- HMDS/Au: Au4f, C1s, N1s and O1s,

- HMDS/TaN: Ta4f, C1s, Si2p, N1s, F1s and O1s.

The XPS spectra and the fit are shown in the Figure 3.17. The Si2p peak is weak on intensity but indicates the presence of Si on the HMDS/TaN sample. The O1s and C1s regions show the presence of C and O in both substrates. As for the FTIR spectra, the XPS data also suggest that HMDS is only present on the TaN samples.

The Si2p region is weak but is visible on TaN as substrate. C1s region is definitively present on both but taking into account the intensity counts the signal is more significative on TaN. The O1s region also is better defined on TaN as substrate. According to the XPS spectra the HMDS is only present on TaN. The spectra fitting is included top right on the HMDS/TaN regions (left side).
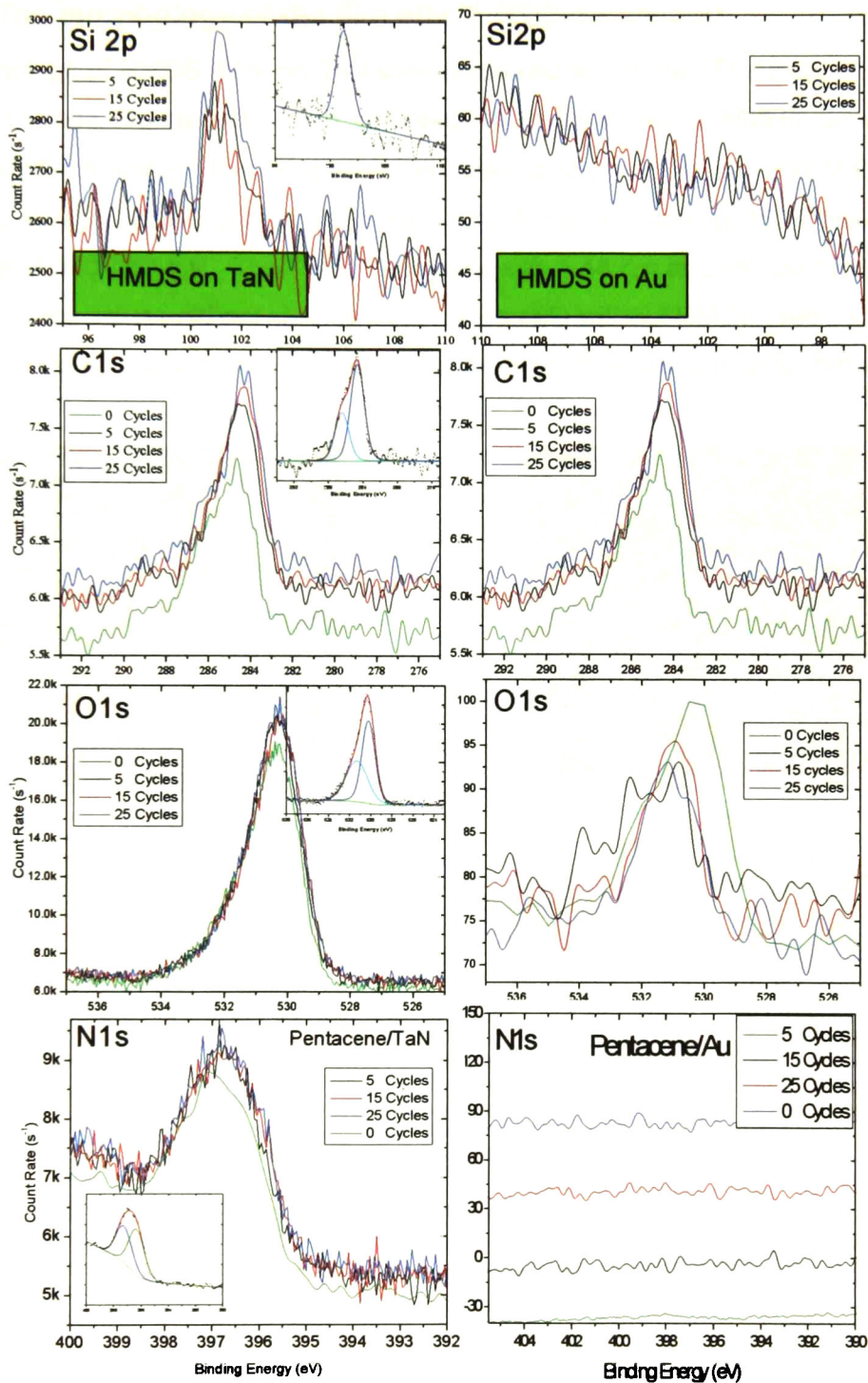
Figure 3.17 XPS Spectra for the samples with HMDS. The left side shows the data for HMDS on TaN and the right for HMDS on Au.

3.6.5. The morphology of the film after HMDS deposition

To morphology of HMDS films on TaN was measured with AFM. The sample employed was S2111 (see Figure 3.9), which corresponds to 25 cycles of HMDS deposition on TaN after HF cleaning. Two magnifications were analyzed (1×1μm and 500×500nm). The data was collected with a scan rate of 0.5 Hz, employing 1024 lines and an amplitude of 360–450 mV. The RMS roughness was 1.44 nm and the average 1.14 nm. Although these values did not change from the sample without HMDS (see Figure 3.14), it is interesting to notice that the morphology looks much more similar to that before the HF cleaning.
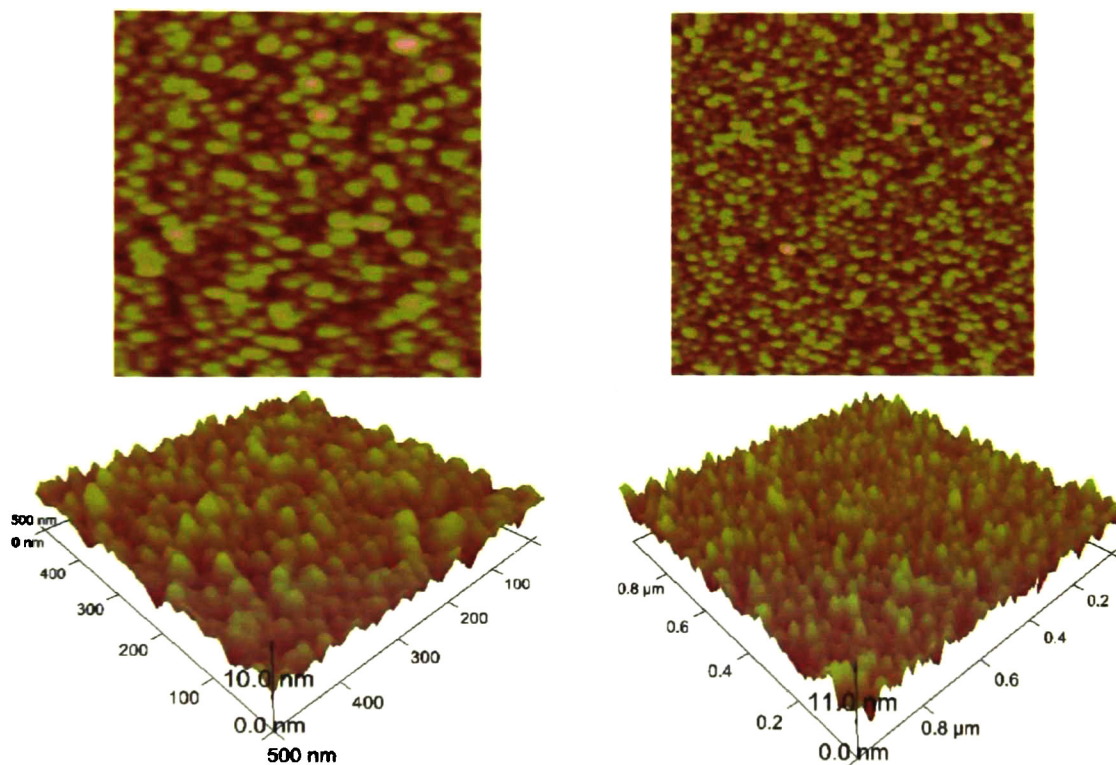
Figure 3.18   AFM image obtained in tapping mode for HMDS (after 25 cycles) deposited on TaN with HF cleaning. The left side shows an image of 500×500 nm area and right side shows an image with of scan size of 1×1 μm. The morphology is different to that of the HF cleaned TaN surface, and is similar to the unclean TaN. The grains do not look uniform.

3.7. Chemical composition

The XPS characterization was performed on Pentacene/Au (Samples: S1121, S1122, S1123, S1124 see Figure 3.8) and pentacene/TaN (Samples: S2115, S2116. S2117, S2118see Figure 3.9). The regions measured were:

- Pentacene/Au: C1s, Au4f and O1s.

- Pentacene/TaN: C1s, Ta4f, N1s, O1s and F1s.

The C1s data and fitting are shown in the Figure 3.19. Three components for C 1s were found for both substrates (Au and TaN). The carbon species considered similar were drawn with the same color. The parameters employed on the fitting including the shift of the C1s respect to the pentacene thickness are shown in the Table 1.9.
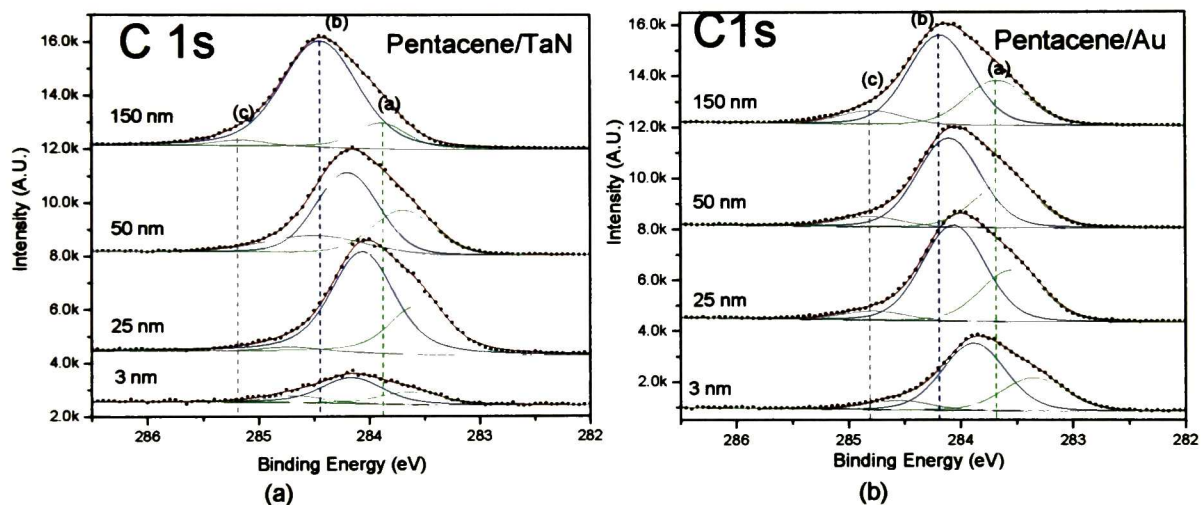
Figure 3.19 XPS spectra. Region of C1s on different substrates (a) Pentacene/TaN (Samples: S2115, S2116. S2117, S2118, see Figure 3.9) and (b) Pentacene/Au (Samples: S1121, S1122, S1123, S1124, see Figure 3.8). There are 3 carbon species on both arrays.

The C1s shift and the intensity on all thicknesses change gradually for both substrates. The Gaussian for carbon determined on Au as substrate was the same for all thickness; for the TaN films the width increased with thickness. The Lorentzian value employed was 0.3eV for all cases. This value was obtained from fit optimization is close to values reported in the literature.[15]

Table 1.9   Fitting parameters for the C 1s XPS spectra for pentacene.

Substrate	BE (eV)	Gaussian	Lorentzian	Peak (Figure 3.19)	BE Shift (eV)
Au	283.35			a	
	284.02	0.51	0.3	b	0.3
	284.77			c	
TaN	283.72	0.53		a	
	284.25	0.56	0.3	b	0.39
	284.82	0.70		c	
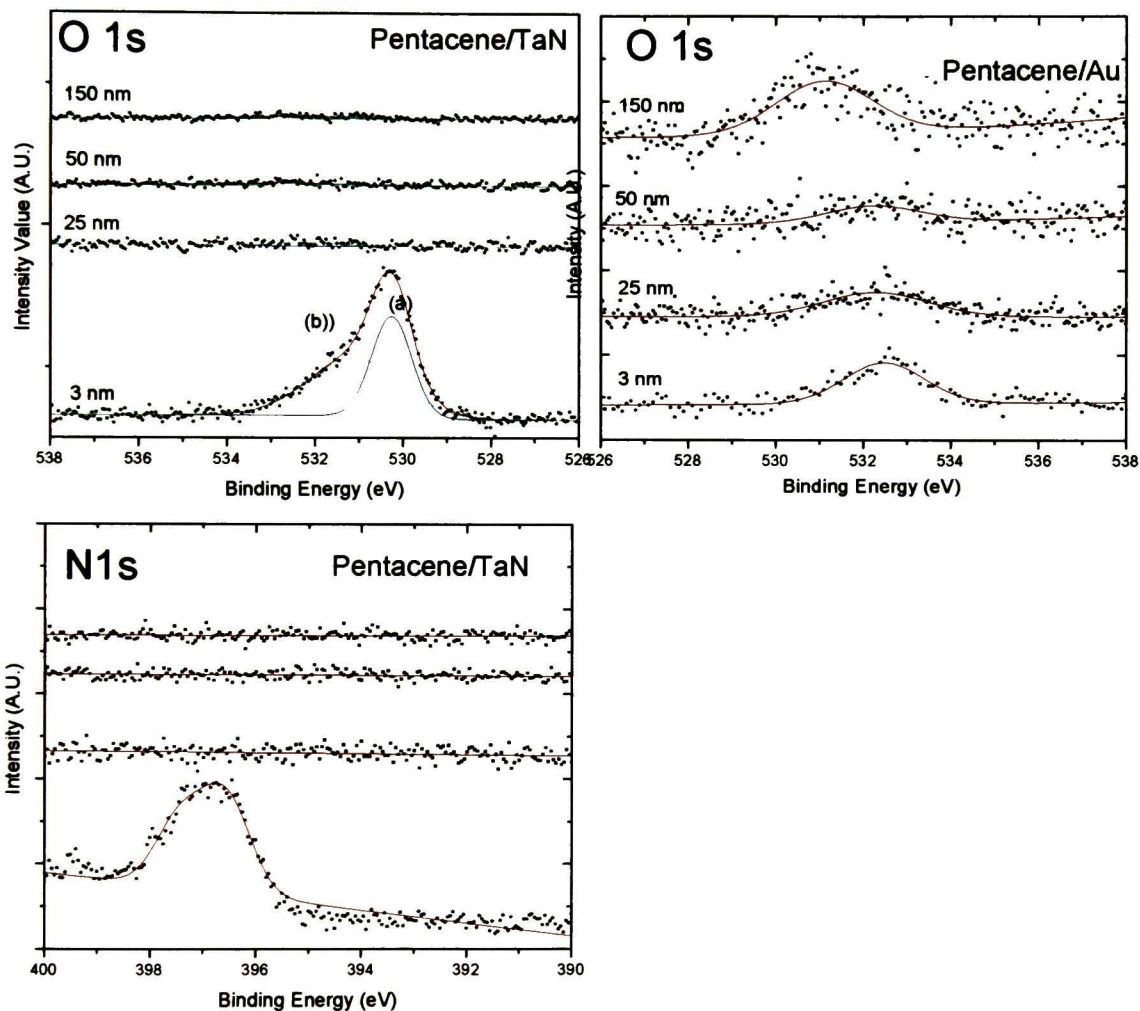
Figure 3.20   XPS spectra for O 1s and N 1s on different substrates. Most of the oxygen and nitrogen in the TaN case was due to the substrate. For the Au substrate, the oxygen position was close to that from UV-Ozone cleaned Au, and shifted gradually to values that might be consistent with oxygen impurities in the pentacene film.

The O 1s data is shown on the Figure 3.20. The parameters employed on the fitting are displayed in the Table 1.10. Most of the oxygen in the TaN case was due to the oxidation of the substrate. The weak signal of the O1s in pentacene/Au had one component.

Table 1.10 Fitting parameters for the XPS spectra for O 1s for pentacene films.

Sample	BE (eV) ± shift	Gaussian	Lorentzian	Peak (Figure 3.20)
Au	532.64	2.35	0.25	a
TaN	531.12	1.73	0.25	a
	531.93	1.99		b

The Figure 3.21 shows the spectra for Ta 4f and Au 4f for the 3nm pentacene film. The data showed no sign for bonding with carbon. The deconvolution for those peaks (one for Au and three for Ta) were assigned to the substrate.
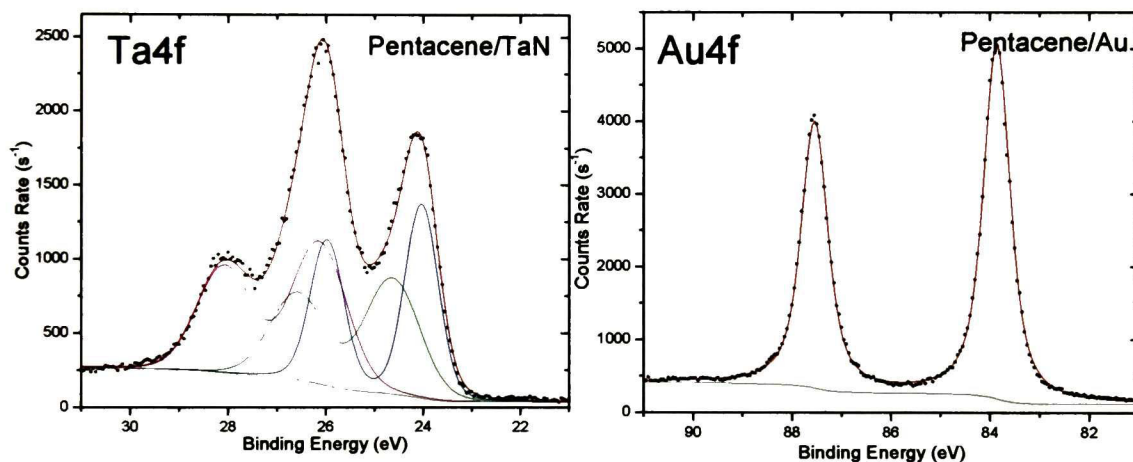
Figure 3.21 XPS spectra Ta 4f and Au 4f for the sample with 3nm of pentacene. There were not signal of C-Au or C-Ta bonds.
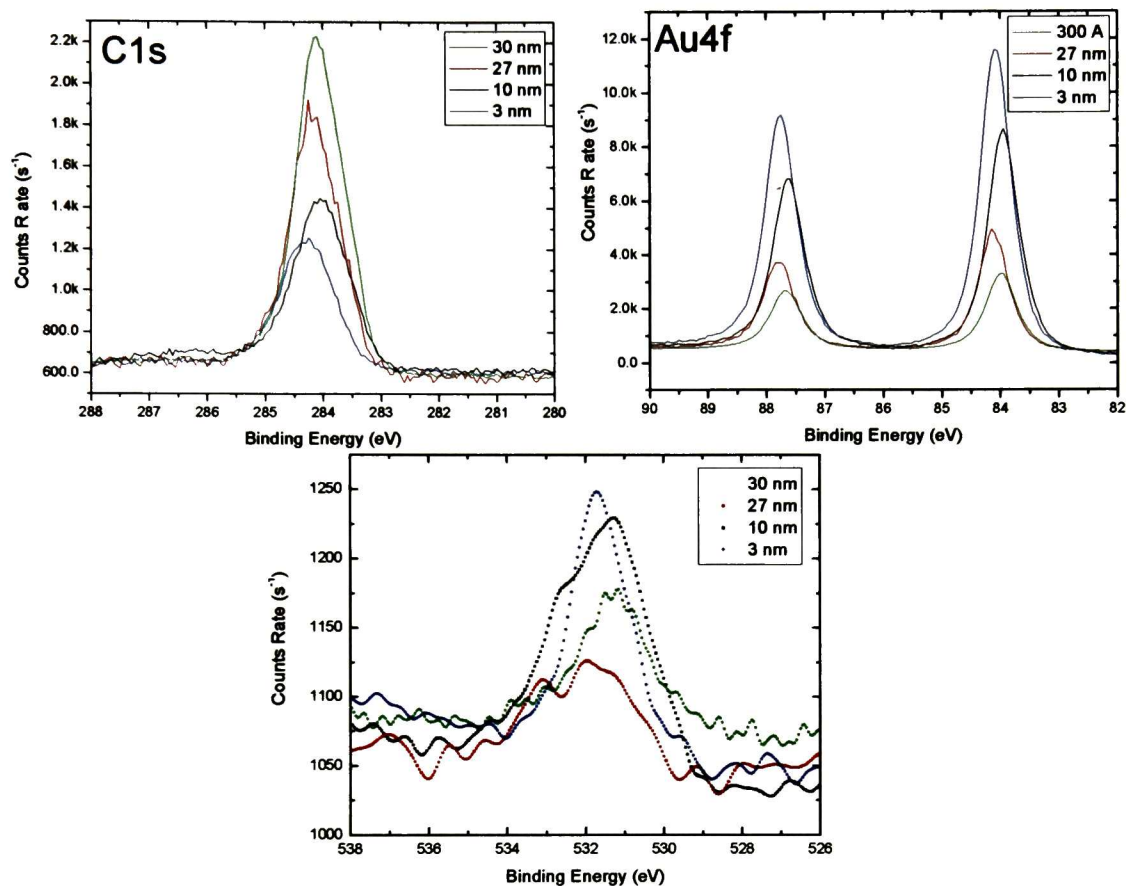
Figure 3.22 XPS spectra Pentacene ($C_{22}H_{14}$)/Au different thickness. Heating the substrate until 55°C. The deconvolution spectra is shown top left of each region. The carbon region (C1s) shows up respect to the increasing on pentacene thickness contrary to gold (Au 4f) region which shows be attenuated. As Oxygen region (O1s) that shows the same behavior as Au4f region.

The Figure 3.22 shows the XPS data of pentacene films of different thicknesses (3nm,10nm, 27nm and 30 nm) grown on Au heating to 55^0C (Samples: S1131, S1132, S1133, S1134). The data for the samples with an HMDS interlayer (Samples: S11115, S11116, S11117, S11118) was very similar and are not shown.

The IR spectra for Pentacene/Au (Samples: S21111, S21112, S21113, S21114, S21115) and Pentacene/TaN (samples: S2115, S2116, S2117, S2118, S2119) were obtained. The spectra comparing the substrates are showed on the Figure 3.23; they

are consistent with those for pentacene shown in the SDBS database.[8] The AFM images in Figure 3.30d clearly show that the amount of pentacene in the nominal 150nm films is comparable for the TaN and Au substrates. However, the IR signal for carbon bonds is much weaker for the Au substrate.
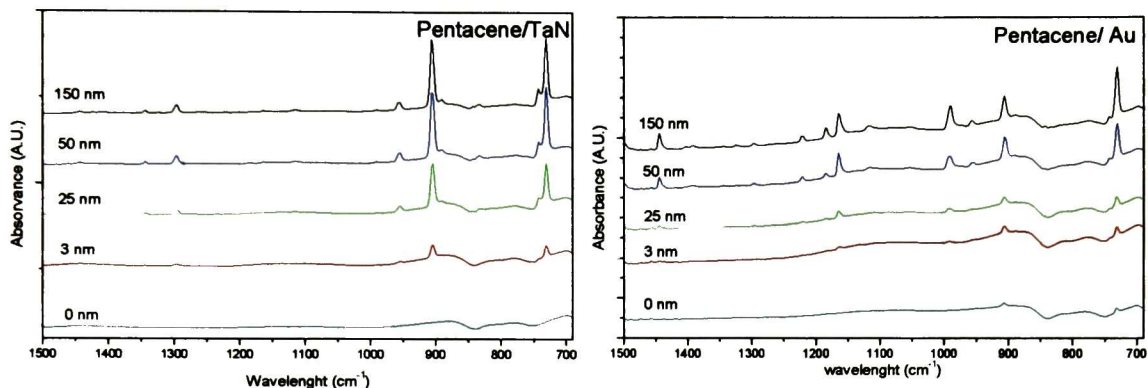
Figure 3.23 IR spectra Region 700-1500 cm^{-1} for films of different thickness grown on Au and on TaN. The peak position and assignation is in Table 1.11 and Table 1.12.

The Figure 3.23 shows that the substrate had a noticeable effect on the FTIR spectra.
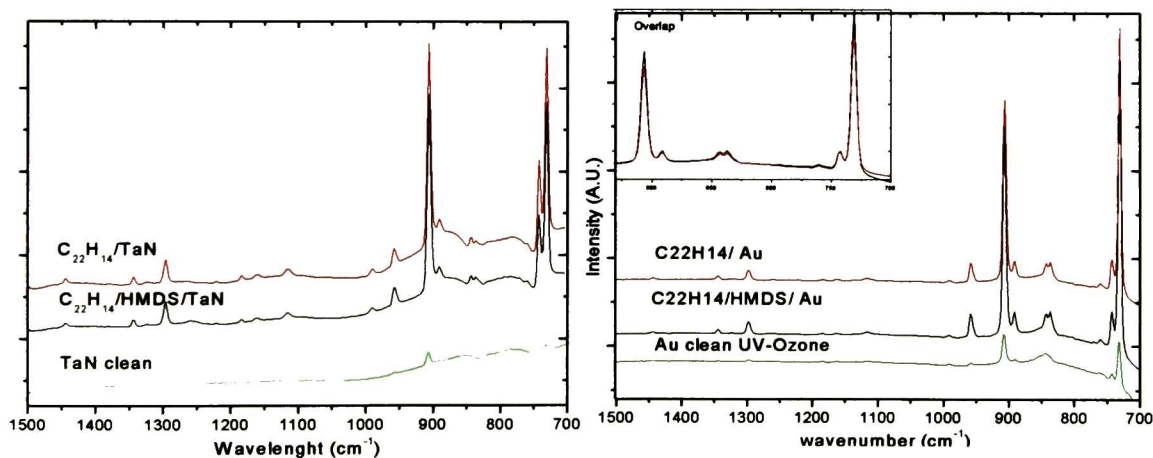
Figure 3.24 FTIR characterization of 30nm Pentacene thick deposited on Au and TaN with an interlayer of HMDS, heated to 55°C during the deposition. The different peaks are C-H bonds of different type.

The IR spectra were obtained from the samples where the substrate was heated to 55°C during pentacene deposition. The samples were pentacene/Au (sample: S1134),

pentacene/HMDS/Au (sample: S11114), Au (sample: S111) and Pentacene/TaN, (S114), pentacene/HMDS/TaN (S21116). The Figure 3.24 and Figure 3.23 show the characteristic pentacene region where C-H and C=C different type are present.

The insert in Figure 3.24 shows that the FTIR signal from pentacene with HMDS (sample S11115) is very similar to that without treatment (sample: S1134). The wavenumber regions of the spectra obtained are described and assigned on the Table 1.11 and Table 1.12. The bonds assignment was based on the chemical environment of the samples (compared with literature) and SDBS spectra of pentacene from Aldrich. The Figure 3.24 shows that the effect of the HMDS interlayer on the FTIR spectra for the films grown on Au was negligible. The same conclusion was found for the films grown on TaN.

Table 1.11   Table of FTIR for pentacene on Au (samples S11115 and S1134) The assignment was based on the database from literature and SDBS spectra of pentacene from Aldrich.[8]

| Sample (label Figure 3.8)	Peaks wavenumber (cm^{-1})	Literature assignment	SDBS database of $C_{22}H_{14}$ presence
1 Pentacene/Au (S1134)	1162.88	Aromatic C-H in plane bend	x
	908.32	Aromatic C-H out of plane bend	x
	777.18		
	730.9		x
2 Pentacene/HMDS/Au (S11115)	1344.16		x
	1297.88		
	958.46	Aromatic C-H in plane bend	
	906.39	Aromatic C-H out of plane bend	x
	890.96		x
	846.75		x
	730.9		x

Table 1.12   Table of FTIR regions assignment samples (S114 and S21116). Database from literature and SDBS spectra of pentacene from Aldrich.[8]

Sample label (see Figure 3.9)	Peaks wavenumber (cm^{-1})	Literature assignment	SDBS database of $C_{22}H_{14}$
Pentacene/TaN, (S114)pentacene/HMDS/TaN (S21116)	1625	C=C: Ar conjugated (note: enhanced intensity)	x
	1296.4		x
	1115.6		x
	957.8	Aromatic C-H out of plane bend	
	906.5	Aromatic C-H out of plane bend	x
	742.5		x
	731.3		x

3.8. The ordering

XRD measurements were performed to determine the pentacene ordering when grown on Au and on TaN, with and without the HMDS interlayer. The samples were

- pentacene/Au: S1121, S1122, S1123, S1124, S1125 (see Figure 3.8).
- pentacene/TaN: S2115, S2116, S2118 (see Figure 3.9).
- pentacene/HMDS/Au: S11111, S11112, S11113, S11114 (see Figure 3.8) and
- pentacene/HMDS/TaN: S21111, S21112, S21113, S21114 (see Figure 3.9).

The X-ray diffraction patterns for pentacene thin films are shown in the Figure 3.25, Figure 3.26, Figure 3.27 and Figure 3.28. The peaks are indexed as (001) reflections in the literature.[16] Some striking observations are the following:

- The pentacene peak for the films on TaN showed up for film thicknesses of 50nm and above.

- The pentacene peaks are different for the two substrates. Both shows two peaks, but are separated by ~ 0.8° for TaN and by ~ 1.5° for Au. The peaks are narrower for the latter.

- It was surprising that the XRD peaks did not show for the pentacene/HMDS/Au samples. At first sight this could be interpreted as the inhibition by HMDS of the ordering for pentacene grown on Au. However, the interpretation could be other if it is considered that the XRD data was obtained in the 2θ mode. In that mode the planes parallel or perpendicular to the substrate do not show up in the XRD spectra. It is then possible that the hydrophobicity caused by the HMDS treatment in turn caused the pentacene molecules to grow preferentially perpendicular to the surface. This would be consistent with the extra features that the pentacene grains show in AFM images (see Figure 3.35).

- There are different reflections centered at different angles according to the substrates. The HMDS attenuates the pentacene ordering when this is deposited on Au as substrate. The HMDS treatment on TaN for 50nm of pentacene helps in the

ordering. The corresponding values for d(001) spacing are shown in Figure 3.29. The x-ray pattern is compared with results of pentacene/SiO_2.[16]

Figure 3.25 X-ray difractogram for Pentacene 150 nm thickness deposited on Au and TaN (black line) and Au and TaN (red line) with HMDS treatment. The different peaks corresponds to different interplanar d(001) distances values.

Figure 3.26 X-ray difractogram for Pentacene 50 nm thickness deposited on Au and TaN (black line) and Au and TaN (red line) with HMDS treatment.

Figure 3.27   X-ray difractogram for Pentacene 37.5 nm thickness deposited on Au and TaN (black line) and Au and TaN (red line) with HMDS treatment.

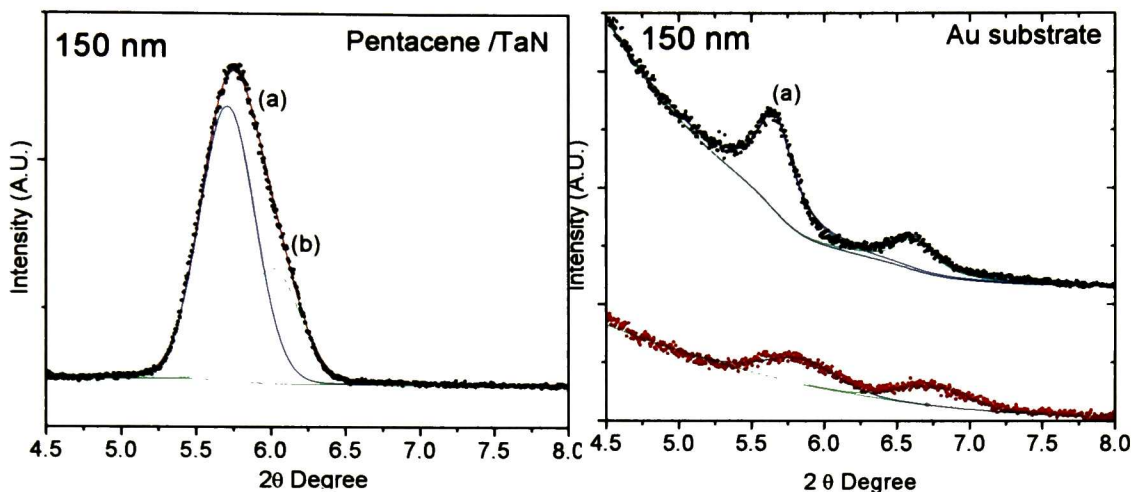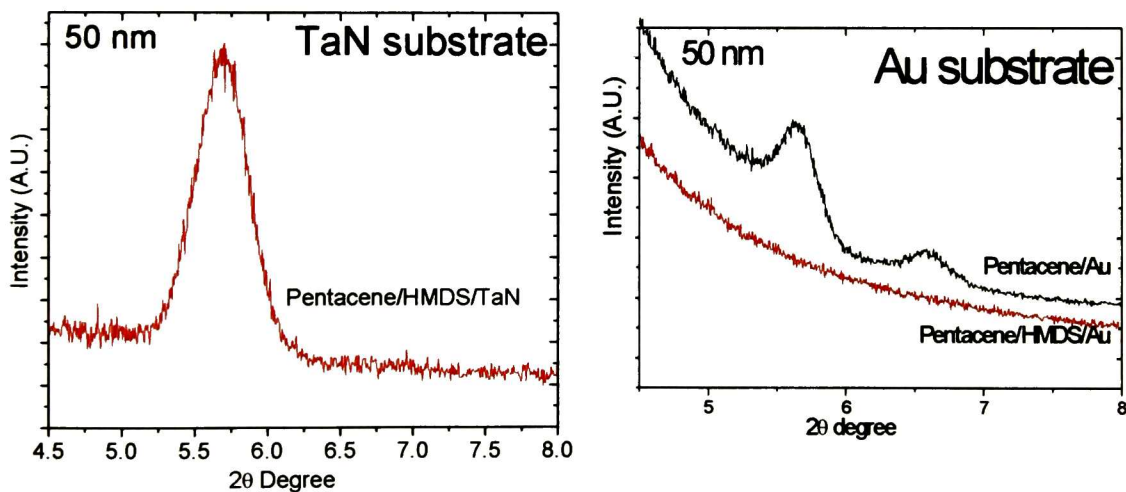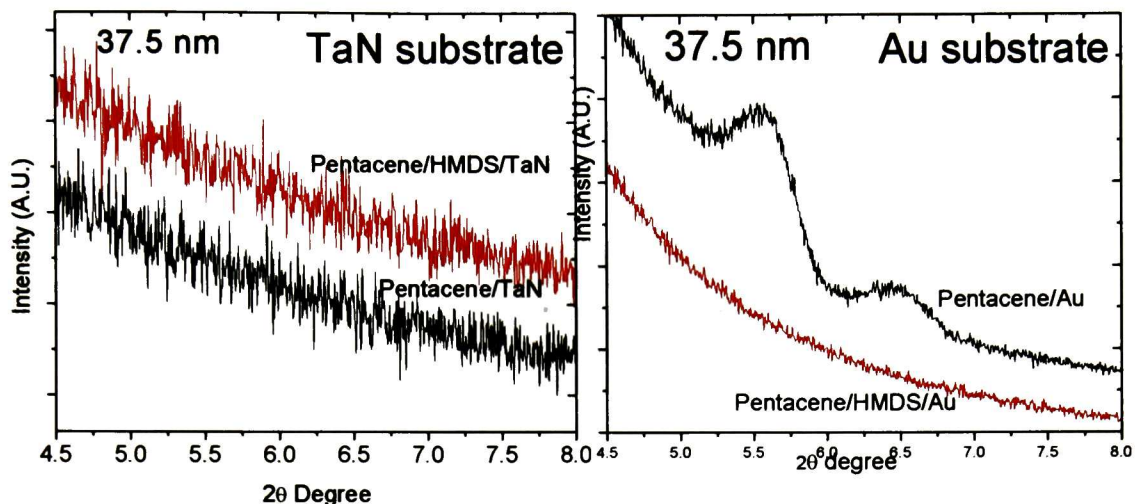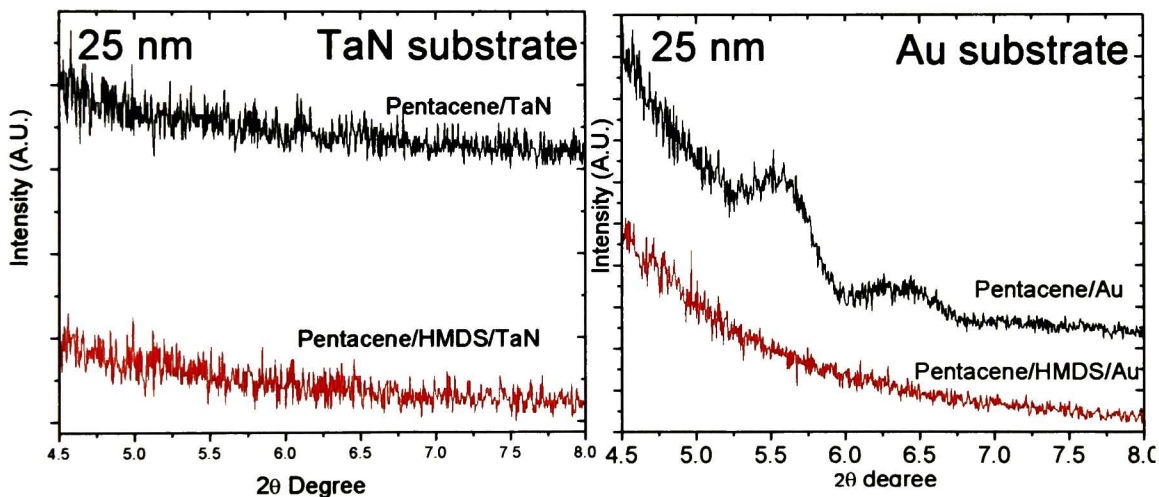**Figure 3.28**   X-ray difractogram for Pentacene 25 nm thickness deposited on Au and TaN (black line) and Au and TaN (red line) with HMDS treatment.
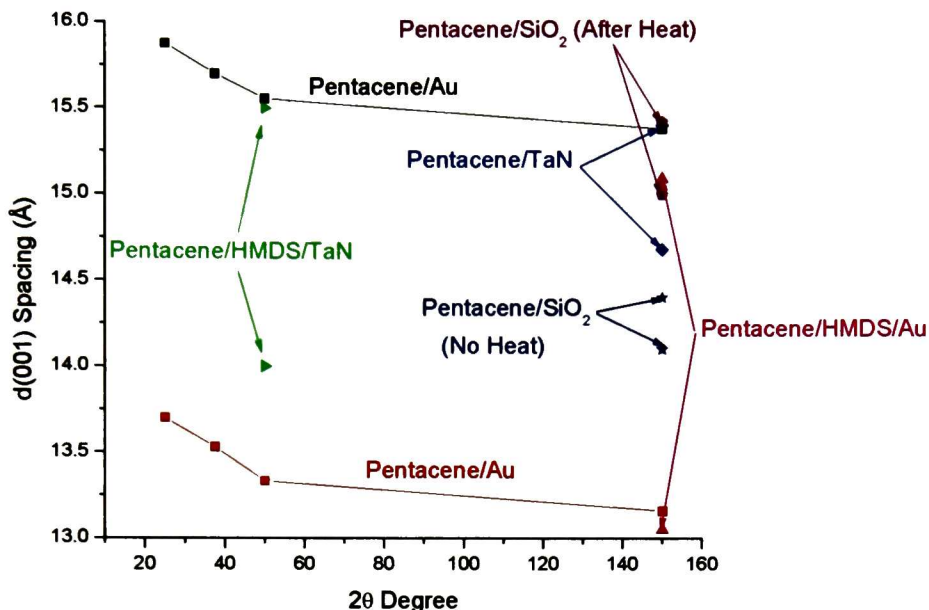
Figure 3.29   d(001) spacing values determined for 150 and 50 nm thickness for thin films of Pentacene grown on Au and on TaN. The values are compared to reports in the literature of pentacene grown on SiO_2.[16] The pentacene/Au peaks showed a clear tendency that could be interpreted as ordering for the thicker films.

The pentacene/Au thin films d(001) spacing showed a clear tendency towards 15Å for the larger polymorph. That could be interpreted as stress relieve since the heated pentacene/SiO_2 is a very stable structure. The samples with 3 nm pentacene films did not show an x-ray pattern.

3.9.   The morphology

AFM studies were carried out on the samples S1121, S1122, S1123, S1124 (pentacene/Au) and on the samples S2115, S2116. S2117, S2118 (pentacene TaN). The AFM images and the roughness are shown on Figure 3.30 and Figure 3.31. The Figure 3.32 shows the morphologies on 500x500 nm area. The scan frequency was 0.59 Hz for all samples. The images were obtained with 1152 lines. The amplitude set point average was 329-350 mV. The approximately time to obtain each image was 45 min.
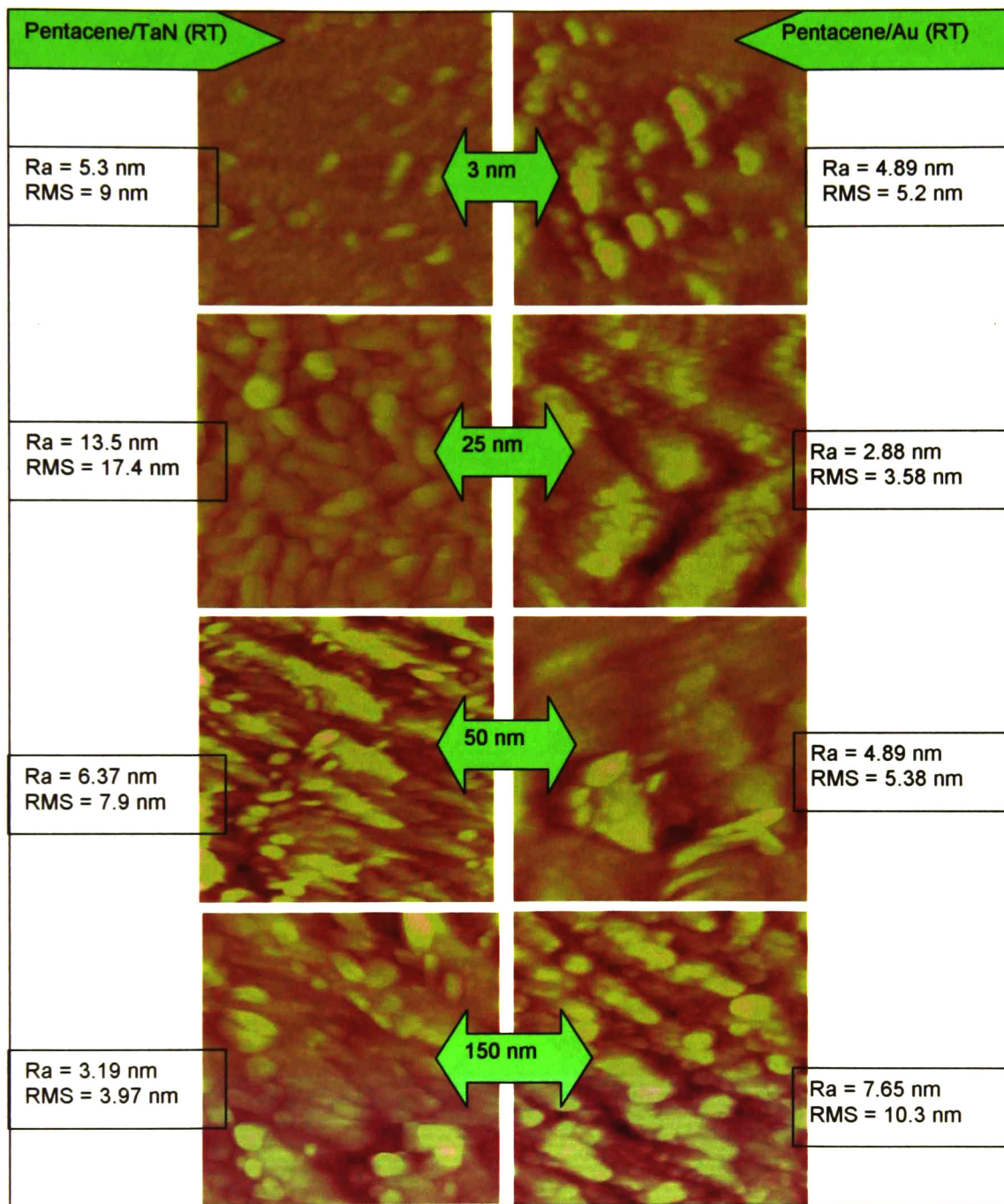
Figure 3.30 Atomic Force images of pentacene films of different thicknesses (nominal 3, 25, 50 and 150 nm) on Au and TaN substrates. The image size is 1×1 μm. The Roughness average (Ra) and Roughness mean square (RMS) are also shown.

Figure 3.31   Same AFM images as in Figure 3.30 but in 3D.

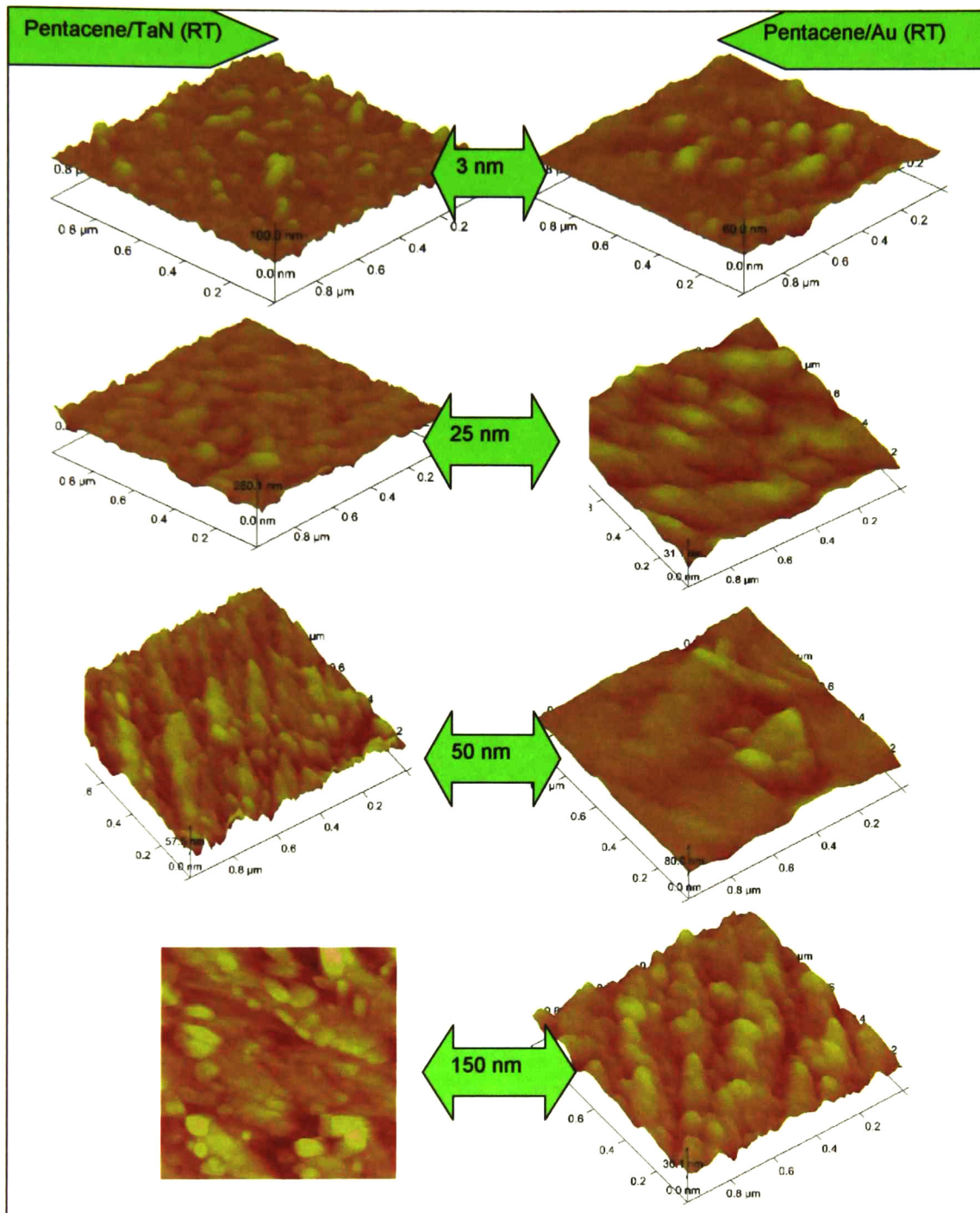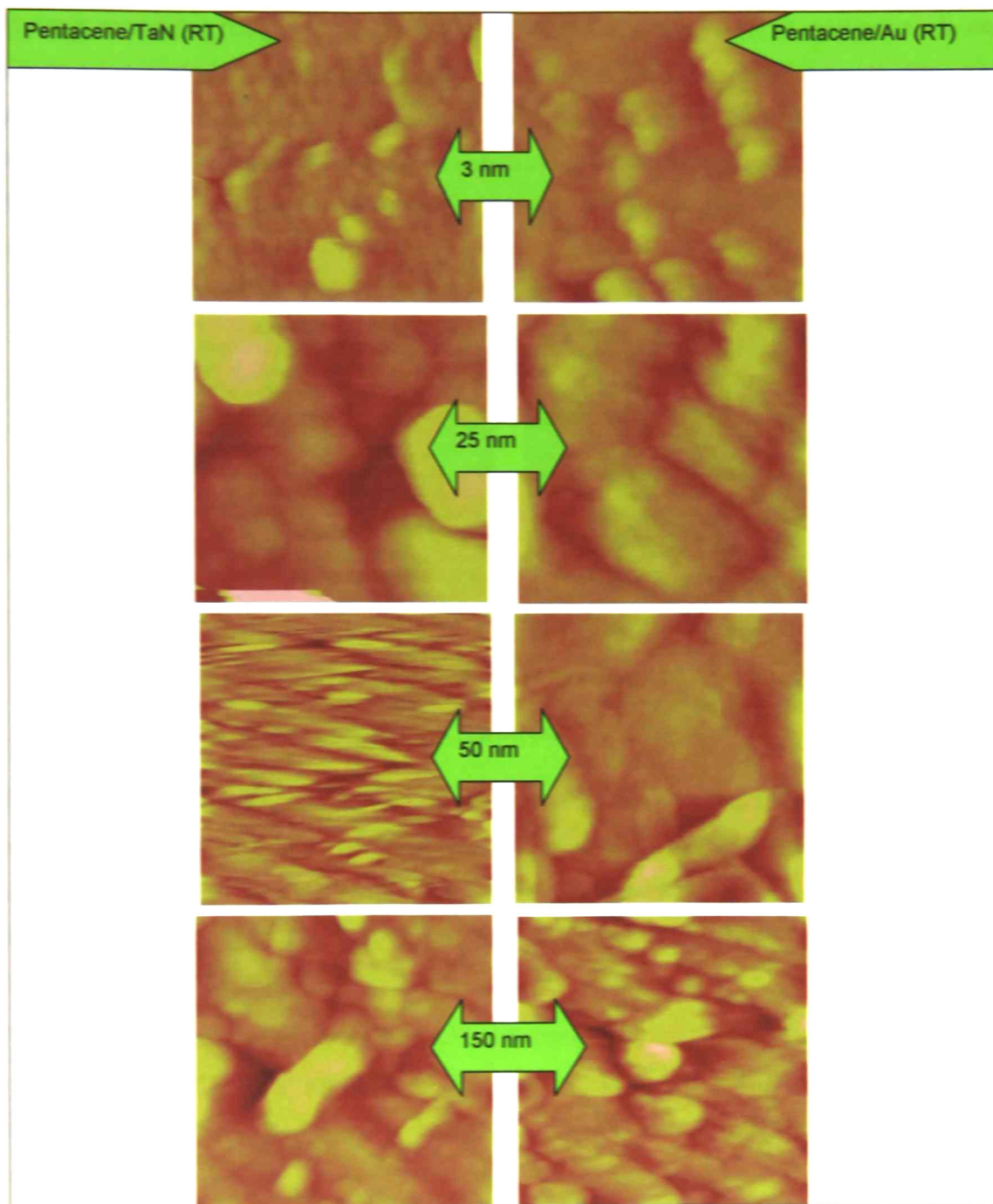**Figure 3.32** Atomic Force micrographs of Pentacene different thicknesses (3,25,50 and 150 nm) on Au and TaN as substrate. The images are observed over the 500×500 nm area. The grain size is visible on these dimensions.

In most cases the roughness was of the same order of the nominal thickness. It was observed a posteriori that the roughness was affected by the exposure to air. The time that the samples expended exposed to air between the film growth and the AFM measurement was not controlled. The substrate holds a clear impact on the pentacene film morphology. Pentacene seems to nucleate with more defined and smaller grains on TaN.

3nm pentacene/TaN   3nm pentacene/Au
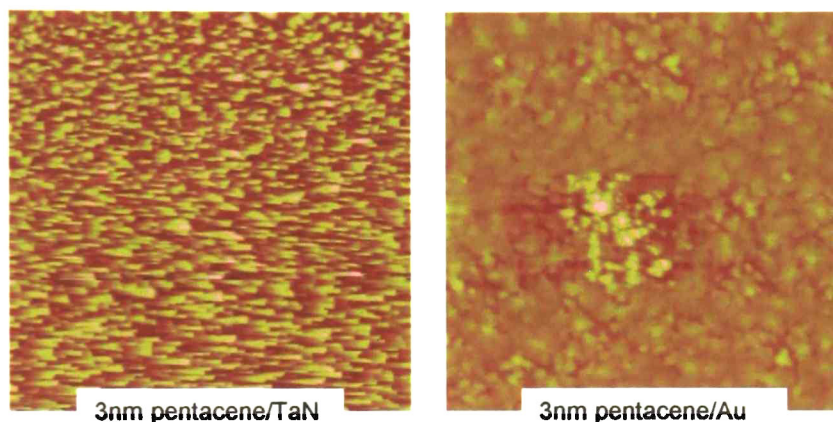
Figure 3.33   Atomic Force micrographs of Pentacene with 3 nm thickness on TaN (left) and Au (right). The images are observed over the 5×5μm area. The Pentacene on Au image shows dendritic grains.

The Figure 3.33 shows that Pentacene of 3 nm thicknesses deposited on Au and TaN with scan area of 5×5 μm. The AFM images were obtained under tapping mode, with scan frequency of 0.59 Hz. The films revealed dendritic grains of pentacene on pentacene on Au. The pentacene on TaN nucleated in scattered points distributed around the surface.

The Figure 3.34 shows the evolution of pentacene films on TaN. The sample was kept in UHV prior to the AFM measurement. The four snapshots were obtained in 40min intervals. The sequence shows a hint of grain growth which could be attributed to the exposure to air.

The morphology of 300Å pentacene/Au films grown at 55°C with (S1134) and without (S11148) a HMDS interlayer is compared in the Figure 3.35. The grains for the film with HMDS were slightly more elongated. The mean square roughness (RMS) was 31.8 nm

and the average roughness (Ra) was 25.3 nm for pentacene/Au. For pentacene/HMDS/Au the values were slightly larger (33.8 and 26.7 nm). The roughness was of the same order of the thickness of the film.

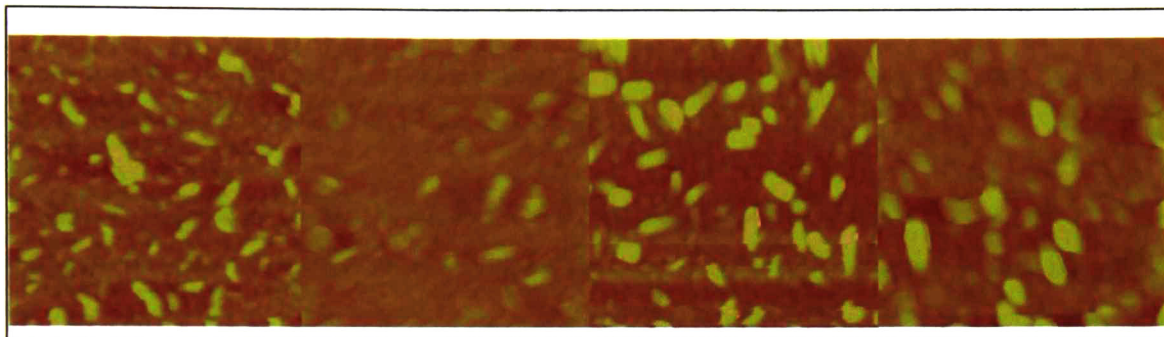**Figure 3.34** Atomic Force micrographs of Pentacene on TaN as substrate with 3 nm thickness. The images are observed over the 1×1µm area. The nucleation is visible. Images are shown according to the measurement time.
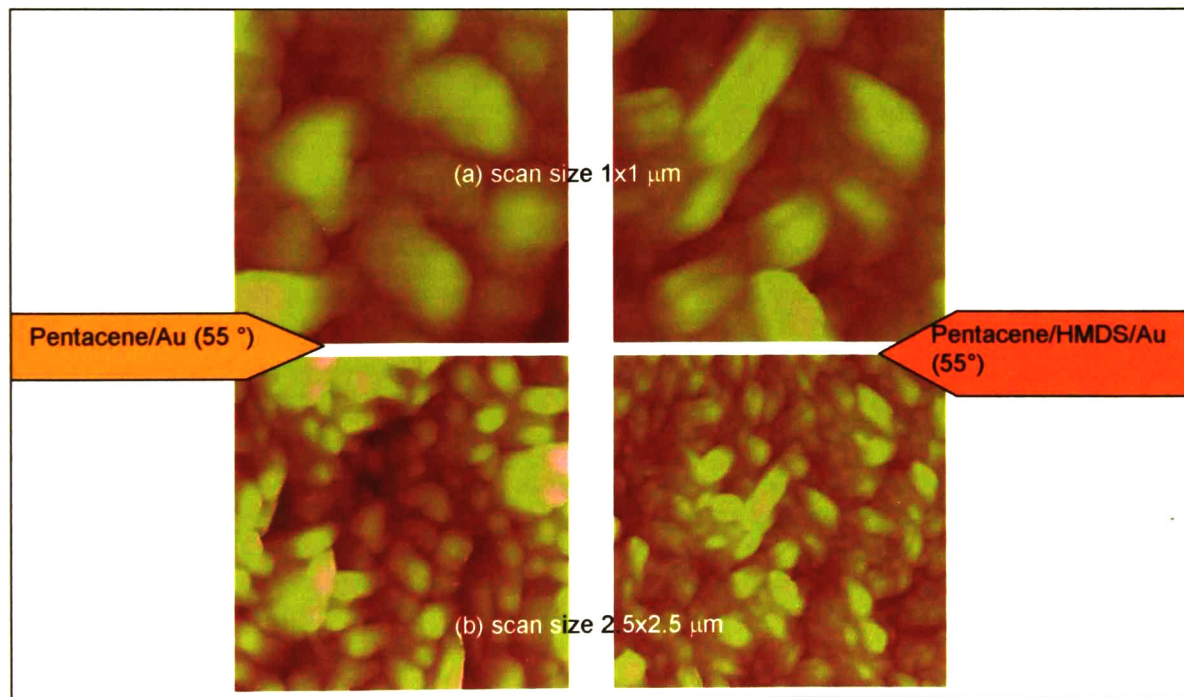

Figure 3.35 AFM images obtained from Pentacene/Au grown at 55°C. There is a hint of columnar-type growth.

The grains for the pentacene/Au case were rounded. For the HMDS case the grains showed lines and were more structured. This could contradicts the XRD images shown in Section 3.8, where the XRD peaks were present for the pentacene/Au films and not present for the pentacene/HMDS/Au films. As discussed in that section, the lack of XRD features could be explained from a preferential perpendicular growth of the pentacene molecules, that is, more ordering.

3.10. The effect of temperature on the pentacene growth

Heating the substrate during pentacene deposition allows for better crystal structure according to results reported in the literature.[16] As shown in the previous sections, the roughness for the films grown at 55°C is much larger that for room temperature growth. Figure 3.36 shows clearly that the pentacene films grown at RT were able to attenuate the XPS signal from the substrate. The large roughness of the films grown at 55°C allowed for the XPS signal from the substrate to show up.
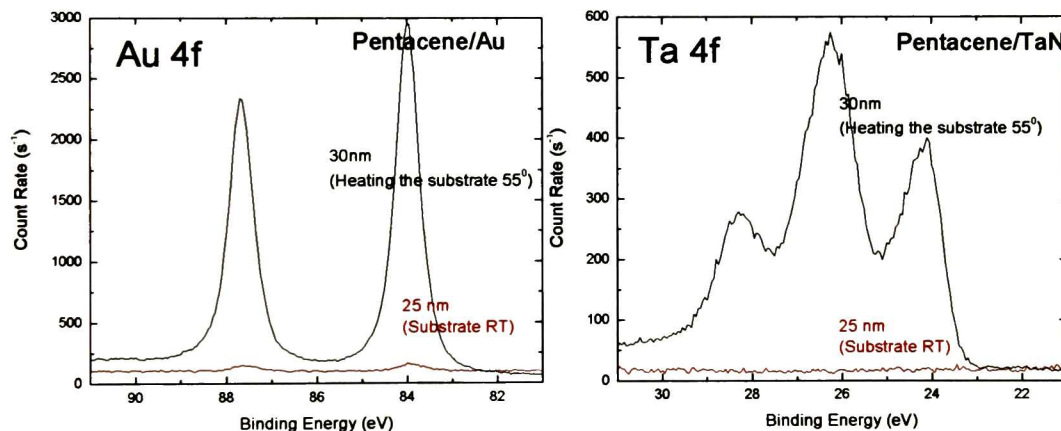
Figure 3.36   a) XPS data of the Au 4f for pentacene/Au grown at RT (S1122) and at 55°C (S1134).   b) XPS data for Ta for pentacene/TaN grown at RT (S2116) and at 55°C (S2114). Although the pentacene thickness were comparable for the films grown at RT and at 55°C, the morphology of the films grown at 55°C allowed for the signal from the substrate to show up.

The temperature affects the roughness, the grain size and the grain features. The effect in the case of pentacene/Au (sample: S1134, morphology showed in Figure 3.35) exposed to the substrate temperature during pentacene deposition, respect to the

sample of pentacene/Au (sample: S1122 and S1123 morphology showed in Figure 3.30) are:

- The roughness increase
- Increases the grain size
- The grain is more defined
- The nucleation is better

At the same time the comparison between pentacene/TaN (sample: S2114, morphology showed in Figure 3.38) respect to the sample that the substrate was not exposed to temperature pentacene/TaN (sample: S2116 and S2117, morphology showed in Figure 3.30) exhibit the next features:

- The roughness increase
- The grain size increase
- The grain is less defined
- The nucleation is not good

The temperature affects the roughness and grain size of pentacene for both substrates, but the grain features and the nucleation are better for pentacene/Au.

It was concluded that the films grown at RT were more uniform than those grown at 55°C.

3.11. Comparison of the chemical structure and morphology of 300Å pentacene/TaN films with and without an HMDS interlayer

Two samples, pentacene/TaN with and without the HMDS layer (samples heating the substrate during pentacene deposition to 55°C; S2114 and S21116), were studied with XPS, FTIR and AFM to find out the effect of the HMDS interlayer on the pentacene structure. The same two samples were also the subject of the ARXPS studies described in Section 3.13. The C 1s data showed no substantial difference on the chemical environment on the sample with (S21116) and the without HMDS (S2114). The same carbon species were present in both cases, although with different ratios. The samples

were exposed to the atmosphere for the same time (approximately the same amount of spurious carbon).
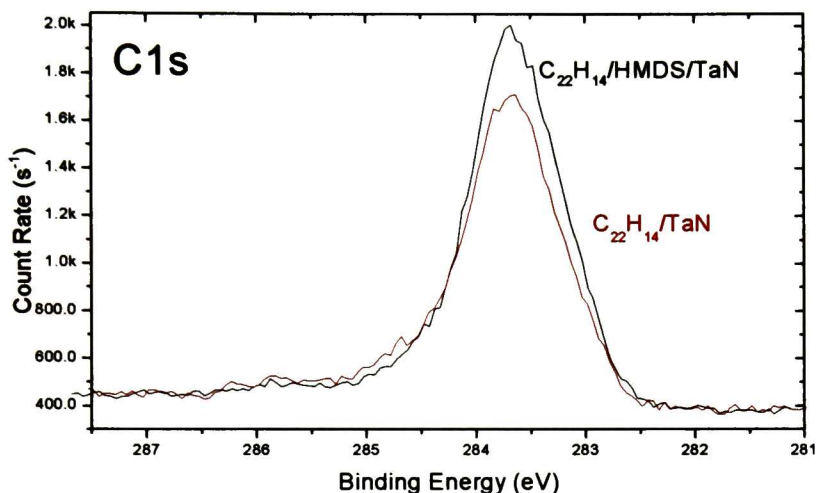
Figure 3.37   C 1s XPS data for the pentacene film on TaN.

The FTIR spectra are shown in the Figure 3.24a for these samples. An overlapping of the IR spectra on samples with pentacene showed no appreciable difference.   The morphologies shown in the Figure 3.38 for both substrates are comparable, although the pentacene/TaN showed more terraces and the pentacene/HMDS/TaN more smaller features.   The RMS in the case of pentacene/TaN was 21.2 nm and for pentacene/HMD/TaN was 13.7 nm.
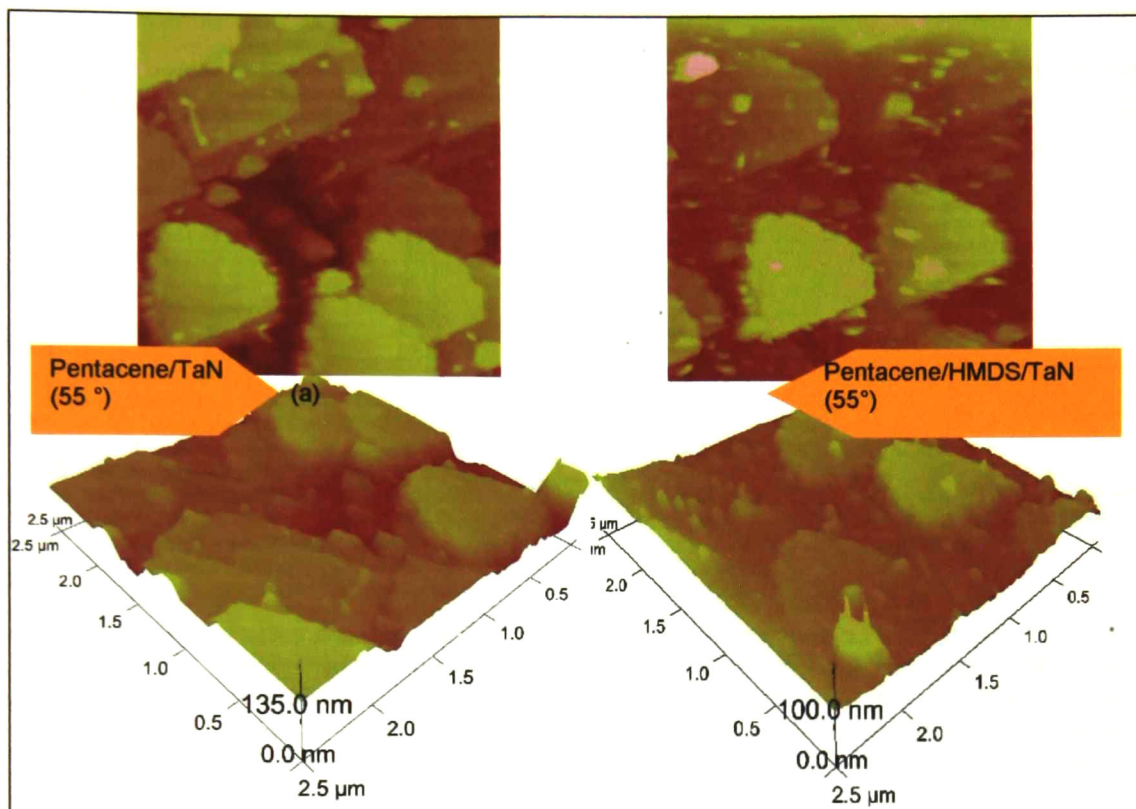
Figure 3.38   AFM scan size 2.5x2.5 µm of (a) pentacene/TaN.(sample: S2114) (b) pentacene/HMDS/TaN (sample: S21116). The morphology was similar among the two samples. The RMS roughness (22nm) was of the order of the film thickness (30nm).

3.12. ARXPS qualitative analysis of pentacene on Au

ARXPS measurements were carried out on 3nm of pentacene on Au (sample S121, see Figure 3.8). Since the roughness was of the order of the film thickness, it was only possible to extract qualitative information. The regions measured were Au 4f, O 1s and C 1s. For Au 4f only one chemical specie was distinguishable (see Figure 3.39a); the Au data showed no evidence of Au-C bond. The dependence of the area with the take-off angle (Figure 3.39b) corresponded, as expected, to bulk Au.

Figure 3.39 Pentacene/Au interface; Au4f region sample No. S121. (a) ARXPS spectra and fitting. (b) Angle- Area dependence. The Au4f region intensity spectra and angle dependence shows a behavior that indicates Au is deep, which is correct according to the chemical environment. The fitting indicates the presence of one chemical Au specie Bulk. Then is not any bond between pentacene and Au.

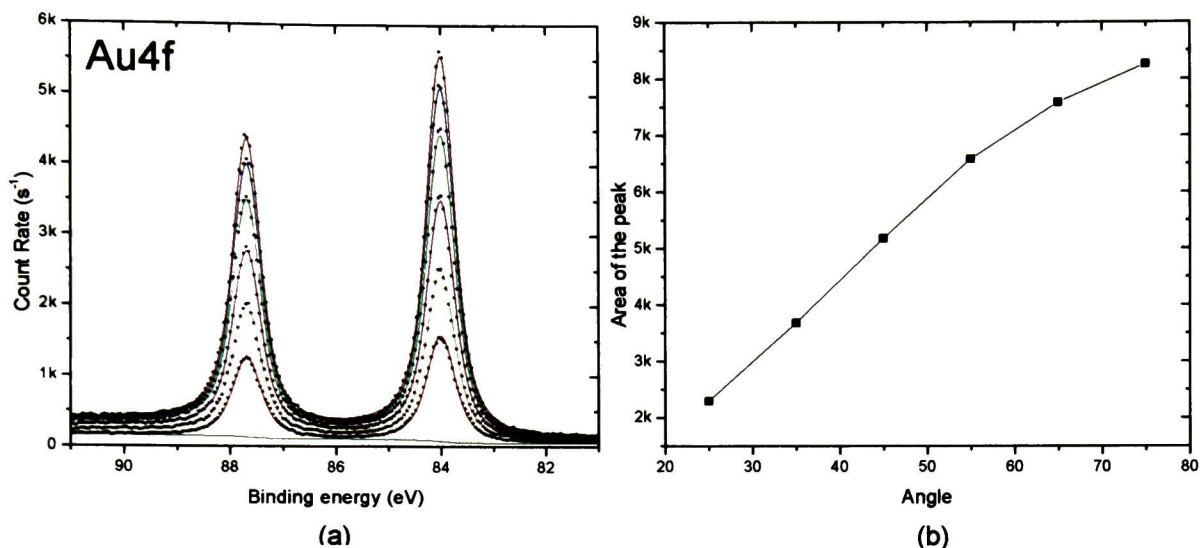The spectra and the fitting obtained for the C 1s is shown on the Figure 3.40a. There were found 3 peaks, which are consistent with those reported in the literature.[17] The peaks as was previously determined correspond to 3 different carbon species. The C 1s spectra were expended and are shown on the Figure 3.40b, showing that the shape of the spectra is identically for all the angles. This strongly suggests that the pentacene was homogeneous and that none of the three components could be assigned to the pentacene/Au interface. This contradicts previous reports that assign Peak-A to the bonding to the substrate.[17]

The spectra for O 1s are shown in Figure 3.41. The strong dependence of the angle peak area on the take-off angle is consistent with the oxygen placed at the pentacene/Au interface. As mentioned previously, the oxygen could be attributed to the UV-Ozone treatment before pentacene deposition. Since there was no evidence of gold oxide, the oxygen might be only adsorbed at the interface.
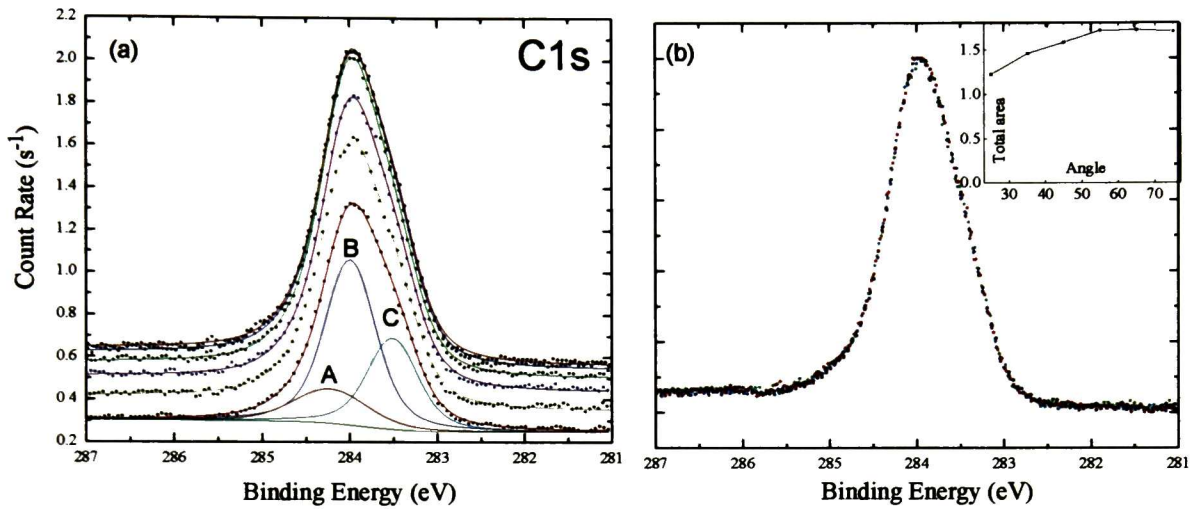
Figure 3.40 Pentacene/Au interface C1s region sample No. 9. (a) ARXPS spectra and fitting. Where there was found 3 different carbon species. (b) Angle- Area dependence. That indicates the different carbon species present through all the thin film.
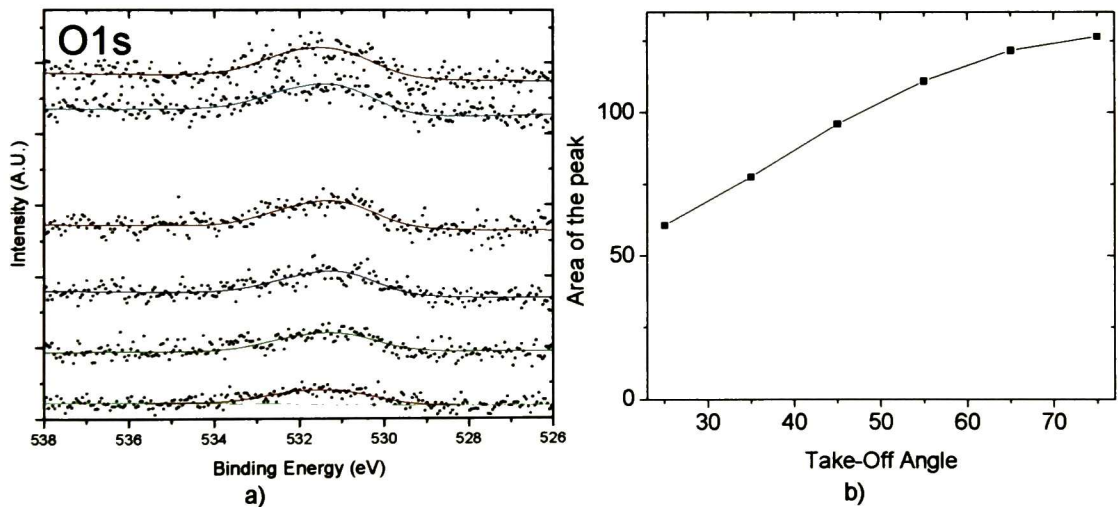
Figure 3.41 Pentacene/Au interface O1s region sample No. 9. (a) ARXPS spectra the intensity is weak the fitting was considered with one peak. (b) Angle- Area dependence tells the oxygen is located on the interface of Pentacene/ Au.

3.13. ARXPS qualitative study of Pentacene/TaN films

ARXPS studies were carried out on 300Å films of pentacene on TaN with and without the HMDS layer (Samples S2114 and S21116). Only the data for the sample with HMDS is shown because the conclusions were very similar. Although the thickness of the film was chosen by mistake (the target thickness was 30Å), this study proved to provide valuable information.

Figure 3.42 XPS pentacene/TaN (Sample: S2114). Ta4f XPS region (a) ARXPS spectra (b) ARXPS spectra and fitting. (c) Angle- Area dependence. The different Ta specie are assigned on Table 1.3. There is not any evidence of Ta-C bond. The Ta$_2$O$_5$ is located through all the film.

The Ta 4f and it correspondent fitting is shown in the Figure 3.42a. It was possible to observe the substrate because the pentacene did not cover the whole substrate surface since the roughness of the film was of the order of the film thickness. The signal from Ta (and N and O) came from the uncovered areas.

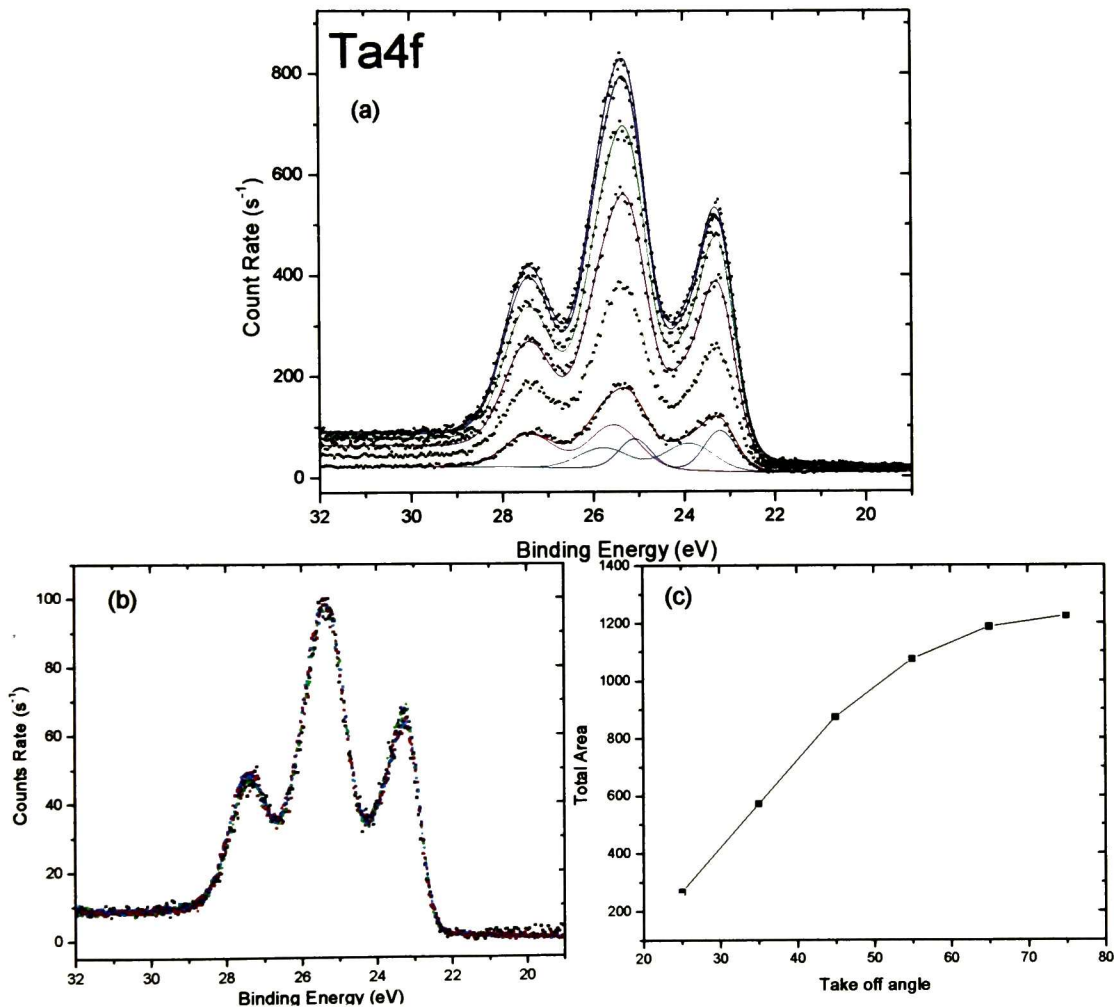As in the clean TaN (see Figure 3.13), there were three Ta chemical species corresponding to Ta_2N, TaN and Ta_2O_5, no evidence of Ta-C bond was found. As it is demonstrated in Figure 3.42b, the shape of the Ta did not change with take off angle. This shows that the three chemical species of Ta are distributed equally throughout the TaN film, at least in the last 60Å. This means that the TaN oxidized component was not located at the TaN surface. Then, either the TaN film was grown from the beginning with a large component of tantalum oxide, or the oxygen from the atmosphere was able to oxidize the whole TaN film. It was for this reason that it was impossible to remove completely the Ta oxide with the HF treatment presented in Section 3.5. This is consistent with an ARXPS study performed on HF cleaned TaN. Those experiment were part of the work of this thesis, but they are not shown since the sample was not properly aligned.

The data for N 1s and O 1s are shown in the Figure 3.43. Similarly to Section 3.5, two N species were found corresponding to Ta_2N and TaN.
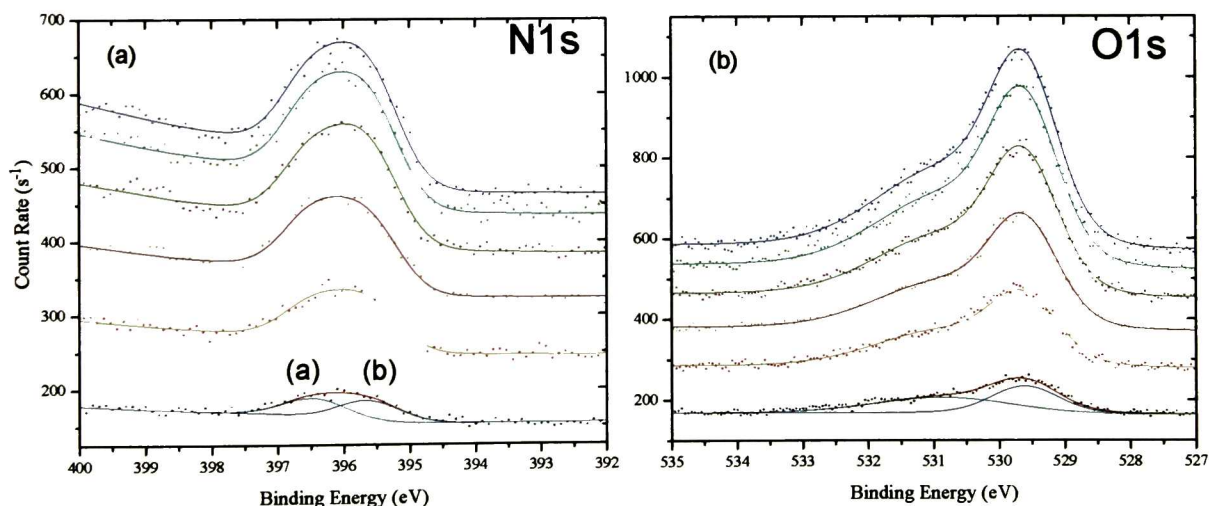
Figure 3.43   ARXPS N 1s and O 1s data for pentacene/TaN (sample S2114).

The C1s ARXPS spectra and the fitting are on the Figure 3.44. The low dependence of the total peak area on the take off angle might be due to the large roughness of the pentacene.
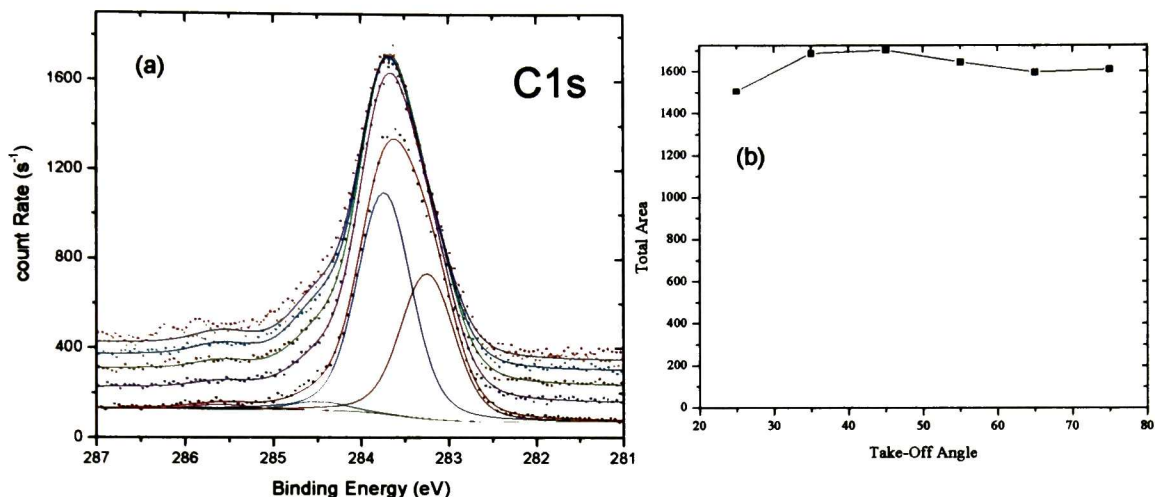
Figure 3.44   ARXPS C 1s data for Pentacene/TaN (sample: S2114).
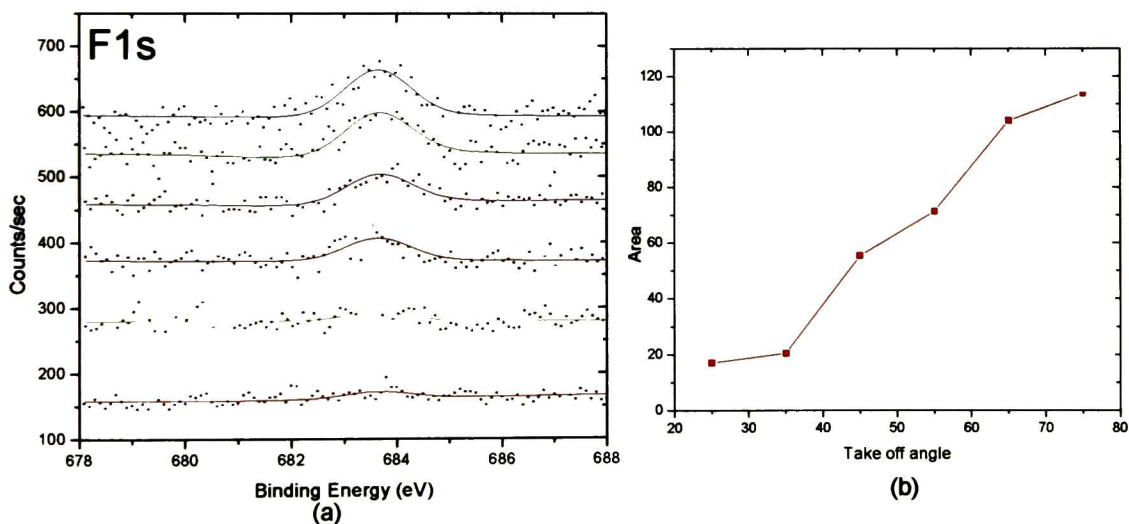
Figure 3.45   XPS of pentacene/TaN (sample: 2114) F1s region. (a) ARXPS spectra and fitting. (b) Angle- Area dependence. According to the slope on angle-area dependence F seems deep on the film.

A weak F 1s signal was detected (see Figure 3.45). The slope of the peak area dependence suggests that the fluorine was deep in the TaN substrate.   This was

consistent with the ARXPS study of the HF cleaned TaN substrate. That study showed that the fluorine was not at the surface.

3.14. The impact of sputtering on the pentacene films

It was desirable to find out the effect of sputtering on pentacene films. The samples employed were S1124 (pentacene/Au) and S2119 (pentacene/TaN), both with nominal thickness of 150nm (see Figure 3.46).
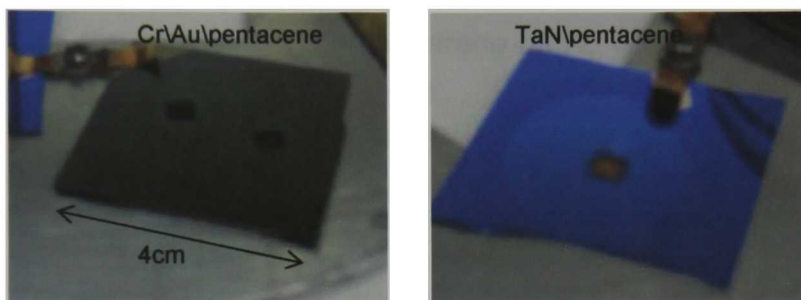
Figure 3.46 Samples of 150nm pentacene films thick after sputtering. The small squares are the 4×4mm area affected by the sputtering. The sputtering also affects the surroundings.
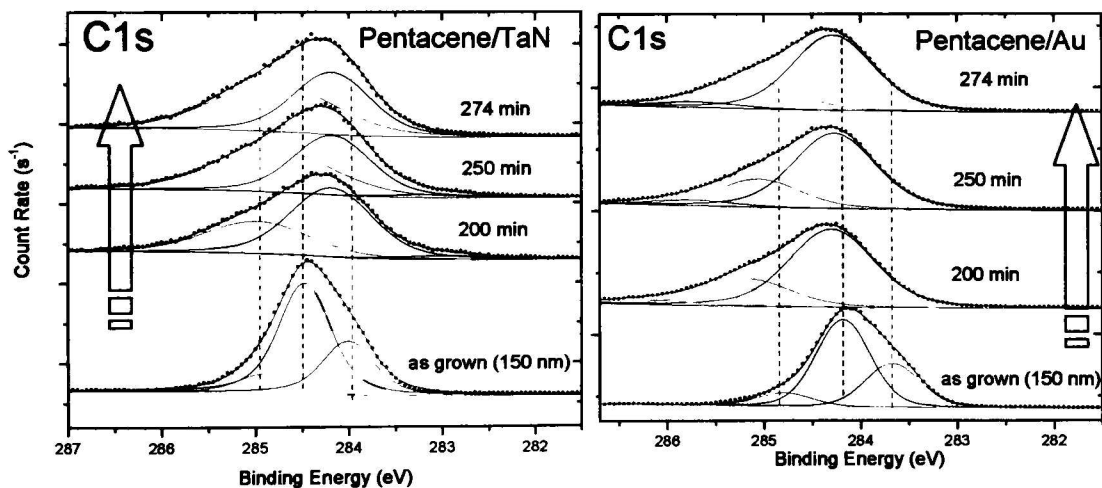
Figure 3.47 C 1s XPS spectra from Pentacene/TaN and pentacene/Au for different sputtering times. The shape started as that for pentacene; the peak widened from the first exposure and did not change shape afterwards.

The Figure 3.47 shows the C 1s spectra for different sputtering times. A widening of the peaks was observed, suggesting that the surface was not longer composed by pure pentacene. This is not surprising since sputtering is considering a destructive technique. The change of shape could be consistent with the transformation of the specie at 284eV into the specie at 285eV.

3.15. The Work Function of the pentacene/Au films

The UPS data of the valence band of pentacene on Au is shown in 0. The samples subjected to the study are listed in Table 1.13.
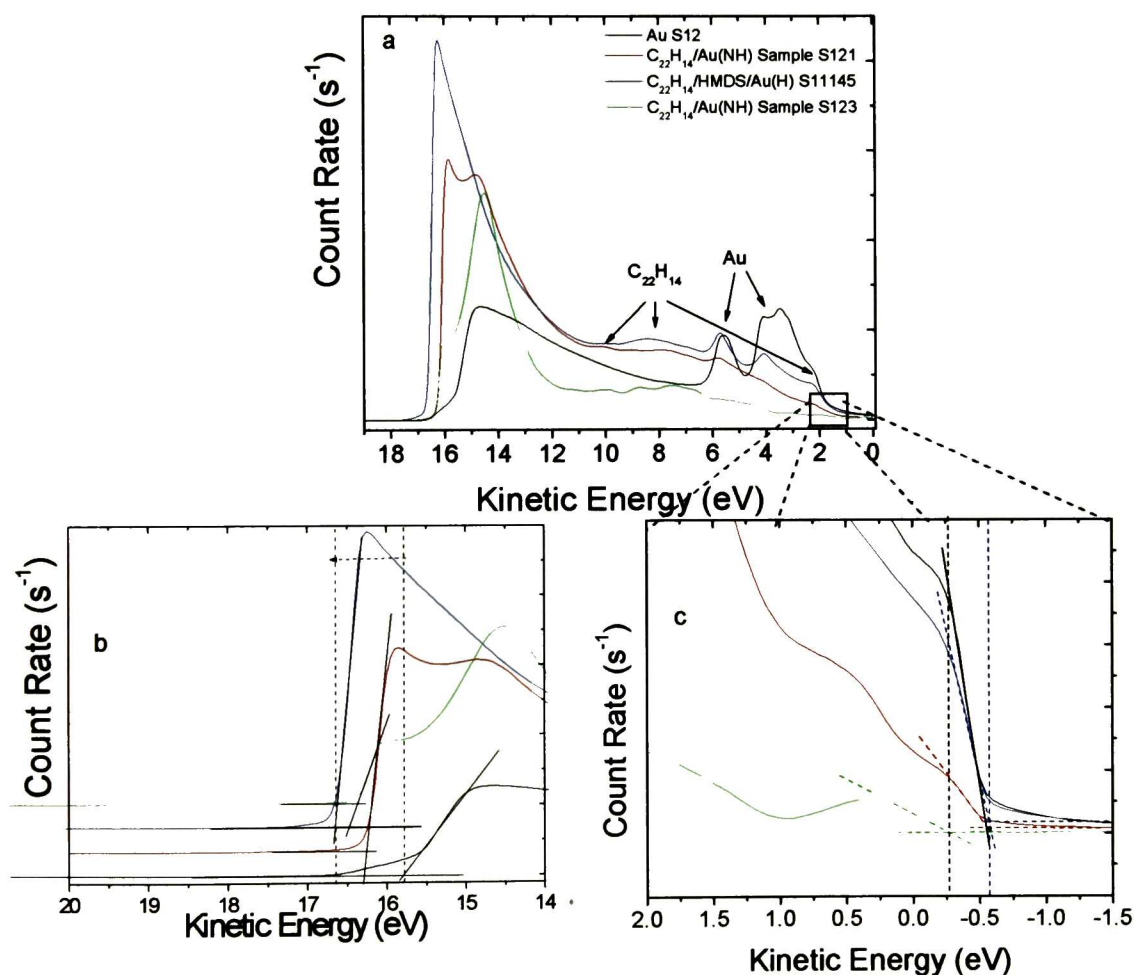
Figure 3.48 a) UPS spectra of the different pentacene depositions on Au including the Au substrate. b) Zoom to observe the cutoff level. c) Zoom to locate the HOMO region.

The peaks at 2.5 and 6eV are characteristic to Au.[18] Those peaks were almost negligible after pentacene deposition at RT, even for the 3nm film (sample S121). However, for the sample deposited at 55°C (S11145) the Au peaks were still visible, even though the nominal thickness of the pentacene film was 30nm. This was consequence of the poor morphology of this particular film and is consistent with the conclusions from Section 3.10. In that section it was showed that the XPS signal from the substrate was still visible for the nominally thick films grown at 55°C due to their large roughness. The small features at 6.6, 8 and 8.9eV are associated to pentacene.[19]

Table 1.13   Samples used in the UPS experiments. The work function was calculated from the UPS spectra. The label of the samples is defined in Figure 3.8 and Figure 3.9. The temperature of the substrate during the growth of pentacene is indicated. When available, the values were compared to reports in the literature. The Au sample was cleaned by sputtering for 4min before the UPS characterization. The evaluation of the work function for the film grown at 55°C is uncertain because the UPS data had contributions from pentacene-covered and uncovered areas.

Sample	Temperature	Work Function (This Work)	Work Function (Literature)
200nm Au (S12)		4.85 eV	5.4,[20] 5.05[21]
30nm Pentacene /HMDS/Au (S11145)	55°C	3.98 eV ?	
3nm Pentacene/Au (S121)	RT	4.39 eV	4.42,[18] 4. 45[21]
150nm Pentacene/Au (S123)	RT	4.55 eV	

The assessment of the cut off and HOMO energies from the UPS data is illustrated in 0 and the values for the work function in Table 1.13. The value obtained for the film grown at 55°C is suspicious since the UPS data had contributions from pentacene-covered and uncovered areas. The rest of the values are comparable to those in the literature.

References

[1]   Muhammad Mustafa Hussain, Naim Moumen, Joel Barnett, Jason Saulters, David Baker and Zhibo Zhang. Metal We Etch process development for dual metal gate CMOS. Electrochemical and solid state letters, 8 (12) G333-G336 (2005).

[2]   Private communication.

3   The method to deposit HMDS, called YES-310 HMDS Vapor Prime Oven Process, was developed at the Erik Jonsson School of Engineering and Computer Science of The University of Texas at Dallas.

4   "AAnalyzer: Un Programa de Análisis para Espectros de Infrarrojo y de Fotoemisión" Alberto Herrera-Gómez. Reporte Interno, Julio de 1998 LIM-CINVESTAV (Registro S.E.P. Número 03-1999-051710412300, diciembre de 1999, México).

5   A. Herrera-Gomez, F.S. Aguirre-Tostado, Y. Sun, R. Contreras-Guerrero, R.M. Wallace, Y. Hisao, and E. Flint. Rapid Communications, Surface and Interface Analysis. In print.

6   "XPSGeometry: A program for depth profile analysis for ARXPS" Alberto Herrera-Gomez, 2006.

7   Robert M. Wallace, Glen D. Wilk. High-k dielectric materials for microelectronics. Solid state and materials sciences, 28:231-285, 2003.

8   T.Saito, K.Hayamizu, M.Yanagisawa and O.Yamamot N.Wasada K.Someno S.Kinugasa, K.Tanabe K.Tanabe and J.Hiraishi and T.Tamura. SDBS No. 11257. *http://riodb01.ibase.aist.go.jp/sdbs/cgi-bin/cre_index.cgi?lang=eng*.

9   Y. Kuo, J. Electrochem. Soc. 139 (1992) 579.

10 K. Sasaki, A. Noya, T. Umezawa, Jpn. J. Appl. Phys. 29 (1990) 1043.

11 Ching-Chung Chang, J.S. Jen, J.S. Chen. Thin solid films 413 (202) 46-51.

12 Joe Daggett, Samuel VillareallC and Roger Robins.UTDallas IC fabrication laboratory HMDS process setup.

13 M.L.P.Silva,I.H.Tan,A.P. Nasciento Filho, E. Galeazzo, D.P. Jesus. Use of plasma polymerized highly hydrophobic hexamethyldissilazane (HMDS) films for sensor development. Sensors and Actuators B. 91 (2003) 362-369.

14 Alexander Tressino de Carvalho, Rodrigo Amorin Motta Carvalho, Maria Lucia Pereira da Silva, Nicole Raymond Demarquette. Hydrophobic plasma polymerized.Hexamethyldissilazane thin films characterization and uses. Materials Research, Vol. 9,No. 1,9-13, 2006.

15 Michelle Alagia, Chiara Baldacchini, Maria Grazia Betti, Vincenzo Cavarreta, Ulf Ekstrom, Carlo Mariani, Stefano Stranges. The Journal of chemical physics 122,124305 (2005).

16 Chistine Corine Matteus. PHD thesis; polymorphism and electronic properties of pentacene. Presented on July 5 2002.

17 Kevin P. Weidkamp,† Christina A. Hacker,† Michael P. Schwartz,† Xiaoping Cao,† Rudolf M. Tromp,‡ and Robert J. Hamers*,† Interfacial Chemistry of Pentacene on Clean and Chemically Modified Silicon (001) Surfaces. J. Phys. Chem. B 2003, 107, 11142-11148.

[18]   P.G. Schroeder, C.B. France, J.B. Park and B.A. Parkinson. J. Phys. Chem. B 107, p. 2253 (2003).

[19]   P.G. Schroeder, C.B. France, J.B. Park and B.A. Parkinson. J. Appl. Phys. 91, p. 3010 (2002).

[20]   N.J. Watkins, L. Yan and Y. Gao. APL 80, p. 4384 (2002).

[21]   F. Amy, C. Chan, A. Kahn. Organic Electronics 6, p. 85 (2005).

Conclusions

- The pentacene films grown on Au and TaN showed three carbon species that are typical to pentacene. There was not evidence of carbon bond to TaN or to Au.

- The pentacene films grown at 55°C had a poor morphology for both Au and TaN substrates. The roughness was of the order of the film thickness. The pentacene thin films (~30nm - 3nm) grew as small islands on the surface; the isles are the cause of the roughness on these films. The UPS and XPS signal from the substrate was visible even for the nominally thick films.

- Although the HMDS treatment did not result on the deposition of a HMDS layer on Au substrates, it had a profound effect on the crystalline structure of the pentacene films. Although the pentacene grains on pentacene/HMDS/Au films are more structured, the XRD peaks were inhibited. The consistency between these two observations could be reached if it is assumed that the orientation of the pentacene molecules was preferential and oriented according to the substrate for films grown on HMDS treated Au surfaces. (For highly preferential growth, the (001) peaks are not observed in the 2θ XRD mode.)

- The HMDS layer had a subtle influence on the chemical and physical structure of the pentacene films grown on TaN. In this case there was not enough data to find out the influence of the HMDS on the crystalline structure.

- The structure of the pentacene films was very different for the two substrates. While in Au the pentacene grew on a dendritic mode, in TaN nucleated around points scattered in the surface. The grains for TaN were larger and more defined. The small grains for Au aggregated to form larger structures.

- The HMDS interlayer did not affect the roughness values of the pentacene films.

- There were at least two pentacene polymorphous in the pentacene films. The different structures determined by the d(001) value for pentacene thick film on TaN corresponds to 15.4 and 14.7 Å and for pentacene on Au are defined as 15.4 and 13.2 Å interlayer distance. For thicker pentacene films on Au, the (001) spacing relaxed to lower values.
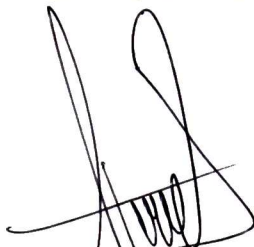
- The ARXPS measurements showed that the Ta_2O_5 component of the TaN substrate was distributed deep into the TaN layer.

- The UV-Ozone cleaning removed the hydrocarbons from the Au surface. The amount of oxygen on the surface increased slightly.

- The HF treatment on the TaN surfaces was more efficient than the SC1 treatment to remove the tantalum oxide. The former treatment smeared the surface grains without affecting the roughness.

- After the HMDS deposition, both substrates showed the same hydrophobicity as measured by Contact Angle.

- FTIR and XPS were consistent about the presence of HMDS when grown on TaN, and about the no presence when grown on Au.

- Approximately one HMDS monolayer was deposited on TaN after 25 cycles.

- The presence of oxygen on pentacene/Au films was attributed to the UV-Ozone treatment. The oxygen was located at the interface.

- The quantitative information that could be extracted from the ARXPS studies was limited because the roughness of the films was of the order of the film thickness. However, valuable qualitative information was obtained. An ARXPS study showed that none of the three carbon component could be attributed to the bonding to the substrate. It showed that most of the oxygen in the pentacene/Au system was at the interface. Other ARXPS study showed that the oxidized component of Ta was not preferentially at the surface, but that it was distributed throughout the TaN film.

- The work function from Au was comparable to the literature values (4.85 eV~5 eV). The pentacene on Au had a work function around 4.4eV.

- The pentacene was stable for at least 24 hours of X-Ray exposure.

Future Work

- To perform XRD measurements at angles that could exhibit the crystalline ordering of pentacene films on hydrophobic Au surfaces (treated with HMDS).

- To control the hydrophobic degree of the Au surface with appropriate treatments and study the pentacene grow mode at low temperatures.

- To study the subtle difference that the HMDS interlayer causes on the pentacene/TaN system by growing pentacene on TaN at low temperatures. (Not enough data was gotten for pentacene/HMDS/TaN grown at RT.)

- To develop a coating that could control the air exposure time since it was found that it might affect the nucleation.

- To perform electrical measurements on films grown at low temperature, and to correlate to the structural properties.

EL JURADO DESIGNADO POR LA UNIDAD QUERÉTARO DEL CENTRO DE INVESTIGACIÓN Y DE ESTUDIOS AVANZADOS DEL INSTITUTO POLITÉCNICO NACIONAL, APROBÓ LA TESIS DE MAESTRÍA LA C. MARIBEL MALDONADO GARCÍA TITULADA: "LA ESTRUCTURA DE PELÍCULAS DE PENTACENO CRECIDAS EN SUBSTRATOS DE Au Y TaN" FIRMAN AL CALCE DE COMÚN ACUERDO LOS INTEGRANTES DE DICHO JURADO, EN LA CIUDAD DE QUERÉTARO, QRO., A VEINTISIETE DE NOVIEMBRE DEL DOS MIL SIETE.

DR. ALBERTO HERRERA GÓMEZ

DR. RAFAEL RAMÍREZ BON

DR. MANUEL ÁNGEL QUEVEDO LÓPEZ

DR. FRANCISCO SERVANDO AGUIRRE TOSTADO

DR. YEVGEN PROKHOROV FEDEROVITCH